Accepted Manuscript

http://dx.doi.org/10.1016/S1090-7807(03)00242-8

Schmedt auf der Günne, J. Distance measurements in spin-1/2 systems by ^{13}C and ^{31}P solid-state NMR in dense dipolar networks. *J. Magn. Reson.* **2003**, *165*, 18–32.

Distance Measurements in Spin-1/2 Systems by ^{13}C and ^{31}P Solid-State NMR in Dense Dipolar Networks

Jörn Schmedt auf der Günne*

Institut für Anorganische Chemie der Universität Bonn,

Gerhard Domagk-Strasse 1, 53121 Bonn, Germany

13*th June*2003

*corresponding author; Email Address: gunnej@uni-bonn.de

Abstract

In this article a solid-state NMR methods for the determination of internuclear dipole-dipole couplings between homonuclear spin-1/2 nuclei are presented. They are suitable for relatively dense dipolar networks which are still dominated by 2-spin interactions. C-/R-symmetry theory is applied to create a double-quantum average Hamiltonian using phase-modulated radio-frequency irradiation and magic-angle sample-rotation. Symmetry derived pulse sequences with improved compensation against chemical shift anisotropies were found assuming a small isotropic chemical shift difference and using numerical calculations of the spin dynamics. Moreover it is shown that a constant time procedure can be used to acquire reliable double-quantum build-up curves even in systems in which damping obscures oscillations in a symmetric build-up curve. This technique is demonstrated on four crystalline model compounds with ^{31}P and ^{13}C spin systems typical for inorganic and biological applications. Comparison to crystal structure data indicates that the distances derived this way from ^{31}P and ^{13}C double-quantum NMR carry only small systematic errors caused for example by anisotropic J-coupling, dipolar contributions from adjacent spins and relaxation.

keywords: NMR, solid-state, homonuclear, dipolar, distance

1 Introduction

Solid-state nuclear magnetic resonance (NMR) may be used as a tool for obtaining structural information in complex disordered molecular solids. Structural information may come in the form of internuclear distances, internuclear angles and, owing to the quantitative nature of NMR, in the form of relative proportions of chemical groups [1]. Many applications to inorganic and organic matter require magic angle spinning (MAS) in order to obtain maximum signal intensity and spectral resolution. Under these conditions structural information is obtained by applying radio frequency (rf) pulses in order to selectively recouple parts of the spin Hamiltonian which otherwise are averaged by the sample rotation. The rf recoupling schemes may be incorporated into multidimensional pulse sequences leading to powerful experiments used for resonance assignment in addition to the already mentioned applications [2–5].

Focussing on techniques which allow to elucidate distance type information there is a wide range of different experimental approaches [3] all making use of the fundamental relationship between the magnetic dipole-dipole interaction and the internuclear distance. This dipolar through-space interaction is related to the dipolar through-bond interaction, the J-coupling, which cannot be used for distance determination by itself. In homonuclear spin-1/2 systems one may classify experiments by the type of spin-operator terms which occur in their average Hamiltonians. For example, average Hamiltonians for RFDR [6] and rotational resonance [7, 8] consist of zero-quantum terms, Hamiltonians for HORROR [9], BABA [10], C7 [11] and R14 [12] consist of double-quantum terms, while for RIL [13], DRAMA [14] and DRAWS [15] average Hamiltonian have contributions from both types. From the type of average Hamiltonian it is possible to derive selection rules which govern the excitation of multispin coherences [16]. Hence, double-quantum average Hamiltonians may be used to efficiently excite double-quantum (DQ) coherences, while zero-quantum average Hamiltonians may be used to excite multi-spin zero-quantum coherences. For spin systems which can be approximated as spin pairs through-space DQ techniques offer advantages as they generally allow the investigation of the coupling of isochronous spin pairs. C7 and R14 are examples taken from the classes of C- [11] and R-sequences [12] developed by Levitt, Nielsen and coworkers, and are different from the other DQ-sequences in the sense that they are dependent on two Euler angles only.

The lower orientation dependence of the average Hamiltonian leads to higher efficiency of the DQ filtered signal.

One common way of determining distance type information using spin-1/2 DQ NMR is based on the acquisition of DQ filtered spectra as a function of the DQ mixing time[1]. This technique has found application in ^{13}C and ^{31}P NMR of inorganic [17–19] and biochemical materials [20–22]. In biochemistry owing to the possibility of selective ^{13}C labeling prominent oscillations have been found, which result in good estimates of distances by numerical simulation of the spin dynamics.

The accuracy of distances stemming from these DQ-experiments depends on the effective suppression of contributions to the spin Hamiltonian other than the required homonuclear dipolar coupling term. In many cases this means decoupling of protons and suppression of the chemical shift interaction. The latter may in principle be achieved by using a low magnetic field and thus scaling down the magnetic field dependent chemical shift interaction. In reality this is often not possible because of losses in resolution, sensitivity or simply because a lower field is not available. If chemical shift terms are not effectively suppressed experimental curves may become sensitive not only to the dipolar coupling constant but also to the chemical shift tensors of the two spins and their relative orientation to the direct dipolar coupling. This problem is in fact more serious in DQ ^{31}P-NMR of inorganic solids than in DQ ^{13}C-NMR of biological samples because of the bigger magnitude of a typical ^{31}P chemical shift anisotropy.

Apart from these complications care has to be taken when further spins come into play or when relaxation is causing a rapid decline of DQ build-up curves. The latter is often true for symmetric [17] ^{31}P DQ build-up curves in inorganic phosphates, thus reducing the available ^{31}P-^{31}P distance information to a qualitative level. In this context it is interesting to note that this can in part be compensated for by the use of constant-time experiments, as was demonstrated on DQ experiments which were used to determine the relative orientation of two chemical shift tensors [23, 24] and for distance determination using a DQ dephasing technique [24].

In this article I present a new approach to measure dipolar coupling constants in systems with relatively big chemical shift anisotropies, using build-up time dependent DQ spectroscopy. The sequences presented here are suitable for systems with relatively dense dipolar-coupling networks

[1]The plot of the intensity of the DQ filtered signal as a function of the DQ mixing time is termed “DQ build-up curve” in this article.

of spin-1/2 nuclei. Primary target systems for this work are the ^{31}P-^{31}P networks of inorganic phosphates but the results can also be transfered to biochemical and organic materials probing ^{13}C-^{13}C dipolar couplings. In phosphates the range of the ^{31}P isotropic chemical shift is smaller than the ^{13}C chemical shift range found in aminoacids, at the same time the anisotropy of the chemical shift tensor can be bigger. Thus from the pool of R- and C-sequences [22,25] symmetries are sought which lead to better chemical shift compensation. Their tolerance towards experimental imperfections i.e. amplitude and phase errors is studied by numerical simulation. In addition the influence of amplitude and phase transients is analyzed theoretically according to a recently published model [22] and compared with experimental data. DQ build-up curves are recorded to determine dipolar couplings, with a DQ constant-time setup. In this way the influence of relaxation is minimized which simplifies data analysis. The proposed experiments are demonstrated on four selected model compounds featuring a range of $^{31}\mathrm{P}-{}^{31}\mathrm{P}$ spin-pair distances of up to 3.56 Å.

2 Experimental Section

2.1 Sample Preparation and Characterization

Four model samples were chosen, namely crystalline $Ag_7P_3S_{11}$ [26], $Na_4P_2O_7$ [27], $Cd_2P_2S_6$ [28] and glycine [29]. The ^{31}P containing samples represent three different types of ^{31}P spin pairs, with respect to the dipolar coupling and the internuclear PP-distance (Table 3). In order to demonstrate that the experiments presented here can also be used in organic and biological materials glycine is used as another test case. From a structural point of view $Ag_7P_3S_{11}$, $Na_4P_2O_7$ and $Cd_2P_2S_6$ have 3, 2 and 1 crystallographically independent positions. $Ag_7P_3S_{11}$ is built from a $S_3P-S-PS_3^{4-}$-group with two different phosphorus atoms with an isotropic chemical shift of 101.4 ppm/92.0 ppm and a PS_4^{3-}-group with an isotropic chemical shift of 103.2 ppm while $Na_4P_2O_7$ features a pyrophosphate group which according to X-ray data contains two crystallographically distinct phosphorus positions. $Cd_2P_2S_6$ is built from hexathiohypodiphosphate units $P_2S_6^{4-}$, the two P-atoms are linked by an inversion center in the middle of the PP-bond.

The crystalline $Ag_7P_3S_{11}$ is identical with the sample used in [17]. 99%-1,2-$^{13}C_2-$glycine bought from Eurisotop and crystalline $Na_4P_2O_7$ (technical grade, 99% purity) from Alfa Aesar were

used without further purification. Crystalline $Cd_2P_2S_6$ was synthesized from the elements (technical grade, 99% purity) by heating a stoichiometric mixture in a quartz ampule to a temperature of $\approx 750\,^{\circ}\mathrm{C}$ for 1 week. The product was identified as crystalline $Cd_2P_2S_6$ by means of EDX and powder X-ray diffraction. All samples were also identified from the isotropic chemical shifts from either ^{31}P or ^{13}C solid-state NMR spectra and comparison to literature values [30–33].

2.2 Solid-State NMR

The ^{13}C and ^{31}P NMR experiments were carried out on a Varian Infinity+ NMR spectrometer equipped with a commercial 2.5 mm double-resonance MAS-NMR probe. The magnetic field strength was 9.4 T corresponding to resonance frequencies of $\nu\left(^{31}\mathrm{P}\right) = 161.42\,\mathrm{MHz}$ and $\nu\left(^{13}\mathrm{C}\right) = 100.29\,\mathrm{MHz}$. Samples were rotated within zirconia spinners. By means of appropriate spacers, the sample was confined to the middle $1/3$ of the rotor volume. A commercially available pneumatic control unit was used to limit MAS frequency variations to a 2 Hz interval for the duration of the experiment.

In order to obtain an optimum signal to noise ratio in the ^{31}P NMR experiments spin-lattice relaxation times T_1 were measured using saturation-recovery experiments [34]. The saturation was realized with a pulse comb of $\pi/2$-pulses of typically $20-40$ pulses with an intermediate delay of $20-50\,\mathrm{ms}$. Results are given in Table 1. Saturation combs are also used in all ^{31}P DQ experiments in order to suppress intersequence echos [17]. For a constant total experiment-time repetition rates of approximately the T_1 value will theoretically result in an optimum signal to noise ratio. Only in the case of $Cd_2P_2S_6$ it was not possible to follow this rule because of the long T_1 values observed. Hence a minimum number of scans was used in combination with a long repetition rate (typically 128 s).

For DQ experiments the probe was tuned by minimizing the reflection of high-power pulses. C-sequences applied a rf nutation frequency of 70 kHz, readout pulses a nutation frequency of 140 kHz on the phosphorus samples under investigation. The pulse phase resolution of the spectrometer is 0.25°.

The NMR pulse sequence used for ^{31}P-^{31}P distance measurements is shown in Fig. 1. Only a single rf channel is involved. All pulse blocks shown involve irradiation at the ^{31}P NMR resonance

frequency.

DQ build-up curves were acquired using the pulse sequence sketched out in Fig. 1, which uses a C-pulse sequence of duration τ_{DQ1} after the relaxation delay to convert z-magnetization into DQ coherence. A second C-block of duration τ_{DQ2} is used to reconvert the DQ coherence into z-magnetization which is read out via a final pulse with 90° flip angle. The C-blocks are incremented only in full C-cycles. The C-cycles are constructed using the $C7_1^3$ symmetry, a C-element $90_0 - 360_{180} - 270_0$ and 2-step super cycle, such that the original $\left[C7_1^3\right]$-block is alternated with a 180°-phase shifted block $\left[C7_1^3\right]_{+180°}$. Explicitly the pulse flip angles and phases (notation: $flip angle_{phase}$) for $\left[C7_1^3\right]$ are given by:

$$
\begin{aligned}
C7_1^3 = \{ \quad & 90.0_{0.0}, \quad 360.0_{180.0}, \quad 270.0_{0.0}, \\
& 90.0_{154.29}, \quad 360.0_{334.29}, \quad 270.0_{154.29}, \\
& 90.0_{308.57}, \quad 360.0_{128.57}, \quad 270.0_{308.57}, \\
& 90.0_{102.86}, \quad 360.0_{282.86}, \quad 270.0_{102.86}, \\
& 90.0_{257.14}, \quad 360.0_{77.14}, \quad 270.0_{257.14}, \\
& 90.0_{51.43}, \quad 360.0_{231.43}, \quad 270.0_{51.43}, \\
& 90.0_{205.71}, \quad 360.0_{25.71}, \quad 270.0_{205.71} \}
\end{aligned}
$$

The $C7_1^3$-sequence with the C-element $90_0 - 360_{180} - 270_0$ is rotor synchronized and needs an irradiation with a nutation frequency being 14 times the spinning frequency.

Coherence pathway selection was done phase cycling the pulse phases only, thus keeping the receiver phase constant. This was done using a cogwheel phase cycle [35] of 12 steps with a difference in winding numbers between the excitation and reconversion block $\Delta\nu_{12} = 3$ and between the reconversion block and read pulse $\Delta\nu_{23} = 1$, which amounts to a $\mathrm{Cog12}(2,5,6;0)$. Thus the pulse phase increments ϕ in the i-th experiment for DQ excitation, reconversion and the read pulse block are:

i	1	2	3	4	5	6	7	8	9	10	11	12
$\phi^i_{exc.}$	0.0	60.0	120.0	180.0	240.0	300.0	0.0	60.0	120.0	180.0	240.0	300.0
$\phi^i_{recon.}$	0.0	150.0	300.0	90.0	240.0	30.0	180.0	330.0	120.0	270.0	60.0	210.0
ϕ^i_{read}	0.0	180.0	0.0	180.0	0.0	180.0	0.0	180.0	0.0	180.0	0.0	180.0

The phase cycle selects the coherence transfer pathways $0 \rightarrow +2 \rightarrow 0 \rightarrow -1$ and $0 \rightarrow -2 \rightarrow 0 \rightarrow -1$ as indicated in Fig. 1, neglecting all coherence pathways which involve coherence orders $|p| > 2$.

An additional 4 step phase cycle realizes DC offset and quadrature image compensation.

Experiments on glycine were done using ramped cross-polarization [36] (contact time 1 ms) and continuous wave decoupling employing a rf field strength of 100 kHz on the proton channel. DQ experiments for glycine use cross polarization, followed by a $\pi/2$ pulse flipping magnetization back into the z-direction, then DQ-coherences are excited using POST C7, reconverted and read out by a final $\pi/2$ pulse. ^{1}H continuous wave decoupling was applied throughout acquisition and DQ excitation and reconversion. For a pulse sequence sketch see [37, figure 1].

2.3 NMR Simulations

The simulations of the spin-dynamics were done using the SIMPSON NMR interpreter [38] published by Nielsen and co-workers. Powder averages were chosen according to the Zaremba-Conroy-Wolfsberg scheme [39] with a number of orientations of 1760 (88 α-, β-angle-pairs x 20 γ-angles) or better. Only exception are the multispin simulations in Fig. 8 with a powder average of 160 orientations (20x8). The integration time step for the DQ simulations was chosen as 1/10th of the shortest rf-unit in the sequence.

Simulations of the chemical shift parameters were done by minimizing the squared difference between experiment and simulation using the MINUIT routines [40] in SIMPSON. The fitting was set up such that it uses an alternative description of the chemical shift parameters δ_{iso}, δ_{aniso} and η with the parameters (i) isotropic chemical shift δ_{iso}, (ii) span δ_{span} and (iii) gravity *grav* defined from the principal axis values $\delta_{11} \geq \delta_{22} \geq \delta_{33}$ by $\delta_{iso} = \frac{1}{3}(\delta_{11} + \delta_{22} + \delta_{33})$, $\delta_{span} = \delta_{11} - \delta_{33}$ and $grav = \frac{\delta_{22} - \delta_{33}}{\delta_{span}}$. In this description the fitting process is more likely to converge for η values around 1 than in the description which is used in SIMPSON by default.

The root-mean-square deviation *r* is given for all chemical shift parameters and dipolar coupling constants ν_{dip} which were obtained from fitting experimental curves and spectra. The parameter is a measure for the deviation between experimental and simulated data and defined as follows:

$$r = \sqrt{\frac{\sum_{i}^{\text{points}} \left(y_i\,(exp.) - y_i\,(sim.)\right)^2}{\sum_{i}^{\text{points}} y_i\,(exp.)^2}} \tag{1}$$

DQ efficiencies given are normalized with respect to the intensity of a one-pulse experiment for ^{31}P and to the intensity from a cross-polarization experiment for ^{13}C under otherwise identical conditions.

Selection rules and the calculation of scaling factors for R- and C-sequences are implemented in a Mathematica [41] script by Levitt and Brinkmann, which is available in the internet (see http://www.mhl.soton.ac.uk) and has been used to determine and study promising pulse sequence candidates (vide infra).

Chemical shift parameters are needed to estimate the influence of the chemical shift on the dipolar-recoupling schemes. Chemical shifts δ in this contribution are given in ppm on a deshielding scale [42]. Parameters for glycine were taken from the literature [29, 43]. For the ^{31}P containing samples chemical shift parameters were determined experimentally. While slow spinning MAS spectra for $Na_4P_2O_7$ and $Ag_7P_3S_{11}$ at spinning speeds of $\nu_r = 2\,\mathrm{kHz}$ and $1\,\mathrm{kHz}$, respectively, can be fitted using a single-spin approximation disregarding the magnetic dipole-dipole interaction, in the case of $Cd_2P_2S_6$ simulation has to take into account also the dipolar interaction. Following chemical intuition the main axis of the chemical shift tensors δ_{zz} was assumed to be oriented along the internuclear PP-axis which is improving the fit between experiment and simulation significantly. Note that at very high ($\nu_r = 23\,\mathrm{kHz}$) and very low spinning speeds ($\nu_r = 2\,\mathrm{kHz}$) the previously reported splitting of the ^{31}P resonance of $Na_4P_2O_7$ cannot be resolved, while in an intermediate spinning regime ($\nu_r = 5\,\mathrm{kHz}$) a splitting of the ^{31}P-resonance was evident (spectra not shown) in full agreement with literature spectra [31,32]. This behavior is probably caused by a complicated relationship between sample rotation frequency and the cross terms of chemical shift and the dipole-dipole interaction. The same behavior was also found and analyzed for a similar system, $Na_4P_2O_7 \cdot 10H_2O$ [44]. From the high speed MAS spectra it may be concluded that phosphorus sites while being crystallographically different have the same isotropic chemical shift values within experimental error. For this reason only one set of parameters is given. Definitions of the chemical shift parameters, i.e. isotropic chemical shift δ_{iso}, the anisotropic chemical shift δ_{aniso} and the asymmetry parameter η can be found in the literature [38].

3 Searching for an Optimized DQ-Sequence

3.1 Pulse Sequences with R- and C-Symmetry

DQ excitation sequences can elegantly be obtained by searching the class of C- and R- pulse sequences which have been described, developed and analyzed using the symmetry theory by Nielsen, Levitt and coworkers [11,12]. For this reason only short descriptions of these pulse sequence classes will be given here, more details may be found in the original literature [11,12] and in a recent review by Levitt [45].

Symmetry theory lays a framework for the prediction of effective Hamiltonians for sequences from the class of rotor synchronized C- and R-sequences. Both C- and R- pulse sequences are uniquely specified by the super cycling scheme, by the three integer symmetry numbers N,n and ν, and by the design of the C- or R-element, which in principle can be any composite pulse inducing a flip angle 2π or π around the x-axis in the rotating frame, respectively. Effective Hamiltonians can be predicted for complete C- and R-cycles which are formed by integer multiples of N basic C- or R-elements which span n complete rotor periods.

The construction of the complete cycle for CN_n^ν- and RN_n^ν-pulse sequences from the basic elements is different. Consecutive C_i-elements are related by a phase increment ϕ which has to be added to all pulse phases of the composite pulse forming the C-element. This phase increment ϕ in radians can be calculated from the symmetry numbers N and ν: $\phi = 2\pi\frac{\nu}{N}$

Complete R-cycles are formed by $N/2$ pairs of RR' elements where R' is the "phase inverted" element. Thus the number of R-elements N must be even. The phases in the R-element can be calculated from the composite pulse phases by adding an angle $\phi = \pi\frac{\nu}{N}$. The element R' is obtained by inverting the signs of all phases in the element R.

NMR interactions are often different in their rotational properties [45, Tables 1 and 2]. Based on these properties prediction of the first order average Hamiltonian can be made by simple selection rules which were derived on the basis of average Hamiltonian theory. Terms of the average Hamiltonian $\bar{\mathcal{H}}^{(1)}_{lm\lambda\mu}$ which get suppressed in the average Hamiltonian of C- or R-cycles fulfill simple inequalities.

$$\begin{array}{cc} \mathrm{C}-\mathrm{class} & \mathrm{R}-\mathrm{class} \\ mn-\mu\nu \neq N\mathbb{Z} & mn-\mu\nu \neq \frac{N}{2}\mathbb{Z}_{\lambda} \end{array} \tag{2}$$

Here l, m, λ and μ are the rotational components of the interactions; l and m are space rank and component; λ and μ are spin rank and component; $\mathbb{Z}$ is any integer number, $\mathbb{Z}_{\lambda}$is also integer but depending on the parity of the spin rank it can become any even integer if λ is even and any odd integer if λ is odd. Note that these selection rules are independent of the composite pulse used for the C- or R-element. Thus symmetries can often be found which suppress all interactions apart from the interaction terms in which the spectroscopist is interested in.

While these selection rules provide information on which terms are symmetry forbidden, information on the magnitude of the terms is supplied by the scaling factor κ. The scaling factor is a complex number and its magnitude is smaller or equal to one. It can be calculated for any $\bar{\mathcal{H}}^{(1)}_{lm\lambda\mu}$ if the composite and the symmetry of the pulse sequence are given. Thus it is possible to suppress further unwanted terms by choosing an appropriate composite pulse resulting in a zero scaling factor. As is shown in detail in the original literature [46] the scaling factor is calculated in the following way,

(*i*) for C-sequences:

$$\kappa_{lm\lambda\mu} = d^{l}_{m0}\left(\beta_{RL}\right) K_{m\lambda\mu} \tag{3}$$

(*ii*) for R-sequences:

$$\kappa_{lm\lambda\mu} = d^{l}_{m0}\left(\beta_{RL}\right) \exp\left\{-i\mu\frac{\pi\nu}{N}\right\} K_{m\lambda\mu} \tag{4}$$

where $d^{l}_{m0}()$ is the reduced Wigner rotation matrix element and β_{RL} is the Euler angle between the sample rotation axis and magnetic field. In both cases the factors $K_{m\lambda\mu}$ are defined with respect to the basic element.

$$K_{m\lambda\mu} = \tau^{-1}\int_{0}^{\tau} dt^{0} d^{\lambda}_{\mu 0}\left(-\beta^{0}\right) \exp\left\{i\left(\mu\gamma^{0} + m\omega_{r}t^{0}\right)\right\} \tag{5}$$

The symbols t^0, β^0, and γ^0 refer to time points and rf Euler angles within the basic element. The

scaling factor κ may be calculated from these equations, using a Mathematica script implemented by Andreas Brinkmann.

The magnitude of the scaling factor may now serve as a property which needs to be maximized for optimum performance. The number of composite pulses which led to improved performance of R- and C-sequences so far is limited. Examples which gave promising results in homonuclear DQ spectroscopy are C$= 360_0$, C$= 360_0 - 360_{180}$, C$= 90_0 - 360_{180} - 270_0$, R$= 180_0$, R$= 90_0 - 270_{180}$ and R$= 60_0 - 300_{180} - 60_0$.

While the choice of composite pulse and symmetry helps to control the short term evolution under the sequence, super cycling may be used to improve long term evolution. Without super cycling the C-/R-cycle is usually repeated several times as specified above. With super cycling modified versions of the basic pulse cycle are alternated with the original cycle. In the context of DQ NMR super cycling with a simple 2-step super cycle has been found advantageous [47]: Single-quantum-terms will be suppressed by repeating the full R- or C-cycle phase shifted by π.

A desirable feature for many pulse sequences is a reduced dependence on molecule orientation. Molecule orientations with respect to the rotor frame are usually given by three Euler angles. In case the pulse sequence is selecting a single term only the magnitude of the Hamiltonian will depend on two Euler angles. This feature is called γ-encoding [45]. If several terms are selected γ-encoding cannot be maintained in general. However under special conditions it is possible that pairs of terms remain mutually identical because a sign change in the spin component is compensated for by a sign change in the space component, so that the average Hamiltonian is still γ-encoded [45]. In homonuclear DQ NMR symmetry based γ-encoded pulse sequences have a theoretical DQ-efficiency of about 20% points higher than non γ-encoded. While γ-encoding is a desirable feature in terms of efficiency, there are certain techniques which use the higher orientational dependence for good [48, 49]. In addition, it should be noted γ-encoding also depends on the choice of the super cycling scheme and special measures can be necessary to preserve γ-encoding as in the case of SC14 [50].

3.2 Suppression of the Chemical Shift

In order to generate a pure dipolar DQ average Hamiltonian, it is necessary to suppress all competing terms including the chemical shift. Since the chemical shift contribution is field dependent, it can

become a serious problem under high-field conditions. On the other hand it may not be possible to change to a lower field for reasons of resolution, signal to noise or simply because a lower field is not available. Thus the design of DQ sequences with improved chemical shift compensation is of considerable interest.

Comparing the ranges for ^{31}P isotropic chemical shifts and chemical shift anisotropies of phosphates with the ranges for ^{13}C of amino acids it becomes obvious that the spread in isotropic chemical shift in phosphates is smaller while the spread in chemical shift anisotropies is often bigger than in amino acids. The idea is to trade compensation against isotropic chemical shift differences for compensation against chemical shift anisotropies.

The strategy followed to this end follows closely the strategy used in ref. [51]. First all γ-encoded C- and R-symmetries were determined using the selection rules given in equation 2 (C-sequences within $N \leq 20$, $n \leq 10$, $0 \leq \nu \leq \frac{N}{2}$ and R-sequences within $N \leq 40$, $n \leq 10$, $0 \leq \nu \leq N$) which are suitable for dipolar DQ recoupling under MAS. The pulse sequences were required to suppress all terms with quantum numbers (l,m,λ,μ) not being $(2,1,2,2)$, $(2,-1,2,2)$, $(2,1,2,-2)$, $(2,-1,2,-2)$, $(2,2,2,2)$, $(2,-2,2,2)$, $(2,2,2,-2)$, $(2,-2,2,-2)$ (dipolar DQ terms), either by the C-/R-selection rules, by magic angle spinning or by coherence order selection via phase cycling. In total $109+135=244$ pulse sequence symmetries were found.

In combination with the composite pulses C$= 360_0$, C$= 90_0 - 360_{180} - 270_0$, R$= 180_0$, R$= 90_0 - 270_{180}$ and R$= 60_0 - 300_{180} - 60_0$ and super cycling by repeating a 180°-phase shifted version in total 1194 pulse sequences can be constructed. Their scaling factors were calculated and all combinations with a low scaling factor, i.e. $|\kappa| < 0.13$ have been discarded. Low scaling factors are unsatisfactory because relaxation will have an increased influence. Note that numerical calculations for different symmetries (Fig. 2) indicate that rf demand $\frac{\nu_{rf}}{\nu_r}$ and scaling factor follow a monotonic relationship if the C-/R-element and the type of recoupled DQ-term are kept constant. Under these circumstances high scaling factors will lead to a high rf demand.

The first order average Hamiltonian for the terms $(l,m,\lambda,\mu) = (2,-1,2,2)$ and $(2,1,2,-2)$ has the form:

$$\bar{\mathcal{H}}^{(1)}_{lm\lambda\mu} = \sum_{j<k} \left(\omega_{jk} T^{jk}_{2-2} + \omega^*_{jk} T^{jk}_{22} \right) \tag{6}$$

where $T^{jk}_{2\pm2}$ are second rank spin operators for the interaction between spins j and k, the details of the recoupled interaction between spins j and k being given in the literature [22]. The factor ω_{jk} is proportional to the product of the complex scaling factor κ and the dipolar coupling constant

$$\nu_{dip} = -\left(\mu_0/8\pi^2\right)\gamma^2\hbar/d^3 \tag{7}$$

where d is the internuclear distance and γ is the magnetogyric ratio. Explicitly ω_{jk} it can be written as

$$\omega_{jk} = -3\pi\nu_{dip}\kappa_{2-122}\sin(2\beta_{PR})\, e^{i\left(\alpha^0_{RL} - \omega_r t^0 + \gamma_{PR}\right)} \tag{8}$$

Here the Euler angles $\alpha_{PR}, \beta_{PR}, \gamma_{PR}$ describe a the rotation from principle axis frame of the homonuclear dipolar interaction to the rotor frame and Euler angles $\alpha_{RL}, \beta_{RL}, \gamma_{RL}$ describe a rotation from the rotor to the laboratory frame.

In order to study and compare the chemical shift compensation it is necessary to define a standard compound. Here the ^{31}P parameters of the pyrophosphate group of crystalline $Na_4P_2O_7$ (Table1) were taken and DQ build-up curves at different magnetic fields for all candidate sequences were calculated, using a constant maximum excitation time of 10 ms and constant rf power $\nu_{rf} = 70$ kHz. The pulse sequences are constructed in correspondence to the sequence in Fig. 1 using the appropriate pulse sequence symmetry and element. DQ build-up curves were obtained by equally increasing the conversion times τ_{DQ1} and τ_{DQ2} and plotting DQ filtered intensity against the DQ excitation time. At this point all pulse sequences were disregarded whose complete C-/R-cycle is longer than 500 μs because the oscillations of their DQ build-up curves will be poorly sampled[2]. The ability of chemical shift compensation can be judged from the difference between an ideal curve, i.e. chemical shift is switched off, and the full simulation including the chemical shift. Comparison of different pulse sequences may be done using the root mean squared difference between ideal and full simula-

[2]Sampling using incomplete C-/R-cycles might even work in these cases. On the other hand numerical calculations indicate that incomplete cycles have inferior chemical shift anisotropy compensation.

tion rms_{DQ}. Note that the root mean squared difference rms_{DQ} can take values bigger than 1 if DQ curves show negative values. The root mean squared difference for low fields will stay close to zero indicating that the sequence is compensated against the chemical shift at this field. For higher fields compensation will be lost which will be reflected in a root mean squared difference $rms_{DQ} > 0$. For even higher fields the root mean squared difference rms_{DQ} will be close to 1 indicating that the filtered DQ-intensity is close to zero. Because of this general trend which was found for all pulse sequence symmetries under study, it is reasonable to define a magnetic field B_{max} up to which a sequence is compensated towards the chemical shift. The maximum field B_{max} here is defined as the highest possible field for which a root mean square deviation is always below 0.1. In other words the higher the B_{max} the better the chemical shift compensation. The best 32 C- and R-candidate sequences are tabulated in Table 2.

Comparing the chemical shift compensation with previously used C- and R-sequences, it becomes clear that the focus on samples with small difference in isotropic chemical shifts, has lead to different C- and R-solutions while symmetries which do well with bigger isotropic chemical shift separation like $C7_2^1$ or $R14_2^6$ have low ranking in this context. A common feature of the high ranking sequences in Table 2 is their huge rf demand $\frac{\nu_{rf}}{\nu_r}$ resulting in low spinning speeds. In fact some of these sequences have an rf-demand higher than 20 and might therefore not be suitable for real world applications. In Fig. 3 curves of the field dependent root mean square deviations are given for the symmetries $C7_1^3$, $C9_1^4$ which will become the first choice in this article in comparsion with successfull known symmetries as $C7_2^1$ or $R14_2^6$. For the latter which are not listed in Table 2 maximum fields B_{max} of 5.1 T and 5.7 T can be reached, respectively. In the case of ^{31}P DQ-NMR phosphate studies the gain in chemical shift compensation is obvious, the same should also hold for ^{13}C DQ-NMR as long as the isotropic chemical shift difference is low. From a descriptive point of view it should be noted that neither the scaling factor κ, the basic C-/R-element nor the type of recoupled Hamiltonian term show a simple correlation with the maximum magnetic field B_{max}.

So far only the magnitude of the chemical shift was considered and it was assumed that the DQ-curves were acquired with the transmitter being set on resonance. In practice this will not always be possible especially if more than one pair of resonances is present. However simulations and experiments (results not shown) prove that the sequences $C7_1^3$ and $C9_1^4$ are still well compensated

against a simple transmitter offset over a range of at least 500 ppm as long as the isotropic chemical shift difference remains small.

3.3 Experimental Imperfections

The above discussion did not include compensation against experimental errors like deviations in rf-amplitude, phase errors and phase- and amplitude-transients. In fact these errors can be quite substantial and need to be considered.

Constant Errors in Rf-Amplitude

Constant errors in the rf-amplitude applied to the DQ sequence are given by e_{amp} which is the relative deviation to the ideal field. For example an e_{amp} of -0.1 indicates that instead of a rf field of 70 kHz, which should have been applied ideally, a rf field of $(70-0.1\cdot 70)$ kHz$= 63$ kHz was applied. Experimentally it is found that DQ-sequences have to be compensated against errors of at least 5% in magnitude. In order to estimate the compensation of the candidate sequences given in Table 2, DQ curves at a constant field of 9.4 T with varying amplitude error were calculated. The deviation from an ideal curve (no chemical shift, no amplitude error) was again evaluated for all candidate sequences (plots not shown). In accordance with previous work [37] it turns out that the amplitude compensation is significantly influenced by the choice of the basic element. Especially the R- and C-elements R=90_0-270_{180}, R=$60_0-300_{180}-60_0$ and C=$90_0-360_{180}-270_0$ give sufficient compensation against amplitude errors. Unfortunately this means that many of the high ranking R-symmetries in Table 2 will be sensitive to amplitude errors. Potential candidate pulse sequences which still need to be considered are: $C7_1^3$, $C9_1^4$ and $R30_2^{14}$, $R20_2^9$. Their simulated reponse to amplitude errors is displayed in Fig. 4.

Round off Errors in RF-Phase

Recently it was noted that γ-encoded R-sequences are sensitive to errors in pulse phase especially if long trains of R-cycles are necessary [22]. In the present case the phase resolution of the spectrometer used is 0.25°. Simulations with variable round off error indicate that while γ-encoded C-sequences are insensitive to round off errors up to several degrees magnitude, γ-encoded R-sequences

will suffer from errors as small as 0.05° at long DQ-excitation times. For this reason only the C-sequences will further be considered. Nevertheless it should be possible to use R-sequences for strong dipolar couplings that result in short DQ-excitation times or on spectrometers which offer higher phase resolution.

Amplitude and Phase Transients

In the simulations above only a relatively weak rf nutation frequency 70 kHz was assumed. In case of single channel experiments focused on ^{31}P-systems one could envisage much better performance at higher nutation frequencies. In fact commercial probes are available which are specified up to 160 kHz. The reason for deliberately choosing a lower rf-field is that the effect of amplitude and phase transients with the above indicated C- and R-elements will spoil DQ-efficiency. Simple experimental tests such as increasing the spinning speed of POST C7 from 10 kHz to 20 kHz and rf amplitude from 70 kHz to 140 kHz while keeping conversion times constant have congruously shown a massive decrease in DQ-excitation efficiency because the building blocks in the pulse sequence get shorter and the influence of phase and amplitude transients bigger. In principle special probes with a switchable Q-factor would be an ideal solution of this problem. While a high Q-factor on the one hand has the advantage of enhanced signal reception, a low Q-factor during the pulse sequence could diminish the destructive influence of phase and amplitude transients.

A more quantitative way of estimating transient influence on the DQ-sequences was proposed in reference [22] for the simple case of a change in pulse phase at time point t'. Using a pick up coil amplitude and phase transients can be monitored with a digital scope (Fig. 5). From these data one can obtain two parameters - the transient decay rate constant λ_{tran} and quadrature transient build-up rate constant λ_Q - which describe the transient characteristics. The transient parameters are defined (taken from [22]) for a single phase change $\phi_1 \rightarrow \phi_2$ of two consecutive pulses by:

$$B_{rf}(t) = B^0_{rf}(\phi_2) + B^{tran}_{rf}(t,\phi_1) - B^{tran}_{rf}(t,\phi_2) \quad t > t' \tag{9}$$

Here B^0_{rf} is the ideal field after the junction of the pulses:

$$B_{rf}^{0}(\phi_2) = B_{rf}\left(\cos\phi_2\,\mathbf{e_x} + \sin\phi_2\,\mathbf{e_y}\right) \tag{10}$$

While the transient contributions[3] have the following form:

$$B_{rf}^{tran}(t,\phi) = B_{rf}^{in-phase}(t,\phi) + B_{rf}^{quad}(t,\phi) \tag{11}$$

with

$$B_{rf}^{in-phase}(t,\phi) = B_{rf}\,\mathrm{e}^{-\lambda_{tran}(t-t')}\left(\cos\phi\,\mathbf{e_x} + \sin\phi\,\mathbf{e_y}\right) \tag{12}$$

$$B_{rf}^{quad}(t,\phi) = B_{rf}\,\mathrm{e}^{-\lambda_{tran}(t-t')}\lambda_Q\left(t-t'\right)\left(-\sin\phi\,\mathbf{e_x} + \cos\phi\,\mathbf{e_y}\right) \tag{13}$$

Here $\mathbf{e_x}$ and $\mathbf{e_y}$ are the rotating frame axes. From the transient parameters λ_{tran} and λ_Q the magnitude A and phase φ of $B_{rf}(t)$ can be calculated, which in turn is used to calculate the B_{rf} in the laboratory frame. The induced voltage U is related to $\frac{d}{dt}B_{rf}$ in the laboratory frame. The induced voltage can be approximated as $U \propto A\sin(\omega t + \varphi)$ in this case because the oscillations at the carrier frequency ω dominate over $\frac{d}{dt}A$ and $\frac{d}{dt}\varphi$. A fitting procedure of the observed voltage from the pickup coil resulted in $\lambda_{tran} = (4.00 \pm 0.05)\,10^6\mathrm{s}^{-1}$ and $\lambda_Q = (2.58 \pm 0.06)\,10^6\mathrm{s}^{-1}$.

Now that the transient behavior is characterized, the transient model can be used to calculate the influence on DQ build-up curves again via the magnitude and phase of $B_{rf}(t)$ at various time points. These calculations are done assuming a piecewise constant pulse amplitude and phase. Converging results were obtained with an even stepwidth of $\approx 30\,\mathrm{ns}$. Following the experimental procedure of tuning the rf amplitude to maximum DQ efficiency, curves for the dependence of DQ-efficiency on a constant error in rf amplitude were calculated for $\mathrm{C7}_2^1$ (Fig. 6). Including transients into the simulations results in a splitting of the optimum rf amplitude, in qualitative agreement with experimental evidence (Fig. 6) . The splitting can also be observed for the pulse sequence symmetries $\mathrm{C7}_1^3$ and $\mathrm{C9}_1^4$ using $90_0 - 360_{180} - 270_0$ as C-element. Moreover the amplitude condition becomes narrower, while optimum DQ-efficiency is dropping. These and further simulations underline that

[3]Note: The formula for the quadrature contribution in the original paper contains a typographic error which has been corrected following a private communication with the authors.

with the C-elements C$= 360_0$ and $90_0 - 360_{180} - 270_0$ the maximum rf power is limited by pulse and phase transients and not by the maximum rf pulse power which can in principle be applied to the probe. However differences between experiment and transient simulations for long conversion times remain, which could be due to the unknown relative orientations of chemical shift and dipolar interaction, relaxation or due to limitations of the transient model.

4 Distance Measurements

4.1 The Symmetric Procedure

The internuclear distance between pairs of spin-1/2 nuclei may be estimated by recording DQ build-up curves using the pulse sequence in Fig. 1. This is done by performing several experiments in which the excitation and reconversion times are varied by taking a different number of full C-cycles. Two different procedures have been presented in the past. A so called symmetric procedure in which excitation and reconversion times are incremented such that $\tau_{DQ1} = \tau_{DQ2}$ which leads to an oscillation in the build-up curve of the form $\left\langle \sin^2(\omega\tau_{DQ1}) \right\rangle$ where $\langle \ldots \rangle$ denotes a powder average. The other method is the asymmetric procedure where either the excitation or reconversion time is kept constant while the other is incremented. The latter leads to build-up curves of the form $\langle \sin(\omega\tau_{DQ1}) \sin(\omega\tau_{DQ2}) \rangle$, where ω can be calculated from the dipolar coupling constant. By simulation good estimates for the dipolar coupling constants ν_{dip} and hence the internuclear interaction have been provided, especially in dilute ^{13}C spin systems.

In ^{31}P DQ NMR build-up curves typically take a less favorable form (Fig. 7 and reference [17]). Even though in the symmetric procedure negative DQ intensity ideally is not expected this is frequently observed even at short excitation times caused by slight misadjustment in the rf-amplitude, huge chemical shift anisotropy etc.. Another problem which is frequently encountered in ^{31}P NMR is the severe damping of build-up curves obscuring any oscillations beyond all recognition. The damping may be discussed in terms of relaxation and the influence of further spins. Nevertheless calculations including more than 2-spins indicate that for short excitation times build-up curves can still be understood within the 2-spin approximation even in cases like $Ag_7P_3S_{11}$ where the nearest neighbor to the spin pair is only a factor of 1.4 further away than the internuclear distance in

the 2-spin system (Fig. 8). In order to improve the modeling of the data different decay functions (gaussian [25], exponential [17, 25], biexponential [22]) have been applied to the simulated 2-spin build curves based on empirical grounds. For poor build-up curves where only a single maximum is clearly visible both the choice of the decay function and the number of extra free variables will influence the fitted value of ν_{dip}. It can be concluded that from these curves more quantitative estimates of dipolar coupling constants and distances as in ^{13}C DQ NMR cannot be drawn, despite the sizeable maximum DQ efficiencies that can be reached (35% for $Ag_7P_3S_{11}$, 34% for $Na_4P_2O_7$, 56% for $Cd_2P_2S_6$).

4.2 The Constant Time Procedure

Recently it was shown that constant time procedures can help to simplify problems generated by the damping in DQ build-up curves. DQ constant-time experiments were set up using DQ RFDR experiments and refocussing techniques [23, 24]. The basic idea is to keep the overall recoupling time constant so that modeling of the damping function can be reduced to a simple multiplication of the simulated DQ build-up curve with a scalar value instead of using a damping function leading to simplified data analysis. Since RFDR is recoupling both chemical shift anisotropy and dipolar terms, distance determination requires additional information on the chemical shift tensors which might not be available. In this contribution the idea of constant time DQ NMR is implemented by keeping the sum of DQ conversion times constant $\tau_{total} = \tau_{DQ1} + \tau_{DQ2}$ allowing the use of the pulse sequence in Fig. 1. This procedure leads to build-up curves of the form $\langle \sin(\omega\tau_{DQ1}) \sin(\omega\tau_{DQ2}) \rangle = \langle \sin(\omega\tau_{DQ1}) \sin(\omega(\tau_{total} - \tau_{DQ1})) \rangle$ where τ_{DQ1} is incremented from zero to τ_{total}. These curves are symmetrical with respect to $\frac{\tau_{total}}{2}$ in the sense $I_{DQ}(\frac{\tau_{total}}{2} - \tau) = I_{DQ}(\frac{\tau_{total}}{2} + \tau)$, hence in principle only half the curve is necessary. In terms of the dynamic range and the oscillation frequency of its build-up curve the constant time procedure gives similar values as the symmetric procedure, while the necessary total length of DQ conversion times $\tau_{DQ1} + \tau_{DQ2}$ is only about half as long. Both short total conversion times and simplified data analysis are features indispensable for distance measurements in ^{31}P DQ NMR.

Experimentally the total conversion time should be minimized to reduce the losses caused by relaxation and to reduce the influence of more distant spins. On the other hand the total conversion

time needs to be long enough to induce a zero crossing in the build-up curve which is necessary for reliable data analysis in terms of the dipolar coupling constant. In figures 9, 10, 11 and 12 experimental DQ constant time build-up curves are displayed for 4 different model compounds. Note that the total conversion times were adapted individually to the expected dipolar coupling constants. The experimental data were analyzed using simulated build-up curves in a 2-spin approximation. Thus the only free parameters in the fitting procedure are the dipolar coupling constant ν_{dip} and a scalar taking care of the damping induced DQ efficiency losses. As expected good overlap between experimental and simulated curves can be obtained without prior knowledge of the chemical shift properties using the supercycled version of $C7_1^3$ with a C-element $90_0 - 360_{180} - 270_0$ at 5 kHz spinning speed (Fig. 9, 10 and 11). The crystalline model compounds feature 3 different ^{31}P-^{31}P distances of 3.564, 2.936 and 2.223 Å. In order to demonstrate the scheme for ^{13}C-NMR and bigger dipolar coupling constants a build-up curve was also acquired for $^{13}C_2$-glycine (Fig. 12). ^{31}P-^{31}P and ^{13}C – ^{13}C distances as measured by this method are summed up and compared to X-ray diffraction distances in Table 4.

Discussion

Distance determinations in relatively dense ^{31}P networks have so far been difficult to conduct in a quantitative way. Here small modifications of traditional DQ NMR have resulted in an increase in the precision of measured distances. Detailed numerical calculations of the spin dynamics have shown the influence of chemical shift compensation, amplitude- and phase-transients and amplitude errors. Essential for the acquisition of reliable build-up curves is that the DQ excitation sequence is properly compensated against the chemical shift interaction. In practice it will be necessary to numerically test if the combination of chemical shift and pulse sequence will in principle be able to provide reliable results. In ^{31}P DQ NMR of inorganic phosphate it was shown that at a magnetic field of 9.4 T these conditions can be achieved by the use of pulse sequences with the symmetry $C7_1^3$ or $C9_1^4$ meaning that optimum chemical shift compensation can be achieved at relatively slow spinning speeds.

Even these extra-measures alone will not result in build-up curves from which dipolar couplings and hence distances can be extracted. However interpretation of build-up curves with respect to dipolar coupling constants is significantly simplified by the use of constant time acquisition procedures replacing symmetric and asymmetric procedures. Owing to the shorter overall DQ conversion time and the simplified analysis highly reproducible values for dipolar coupling constants can be determined. Nevertheless the contribution of additional spins to the experimental dipolar coupling constants remains sizeable. From the influence of the closest adjacent ^{31}P spin (Table 3) in terms of the quotient $\frac{d_2}{d_1}$ (d_1 wanted $^{31}\mathrm{P} - ^{31}\mathrm{P}$ distance; d_2 distance of the spin pair to the closest adjacent spin) it may be suspected that the biggest deviations between distances from DQ experiments and x-ray diffraction occur in the case of $Ag_7P_3S_{11}$. This is consistent with experimental findings which indicates that in case of $Ag_7P_3S_{11}$ build-up curves can no longer be interpreted in the 2-spin approximation only.

In this contribution root-mean-square values are given to qualify the deviation observed between experimental DQ constant-time curves and the fitted curves (see captions to figures 9, 10, 11 and 12). It is therefore interesting to see how the root-mean-square deviation in the ideal case reacts onto a deliberate error in distance (Figure 13). This function depends on both the internuclear distance d and the sum of DQ conversion times τ_{total}. From the curves presented in Figure 13 it may be concluded that in the ideal case, i.e. a 2-spin system without chemical shift and experimental errors, a root-mean-square deviation of 0.1 corresponds to an error of about 1.7% in distance. Thus in principle distances determined by DQ constant-time NMR should carry very small statistical errors. However experimental imperfections have a significant contribution, as can be seen for the confidence interval of the experimental PP-distance in $Ag_7P_3S_{11}$ ($d = (3.32 \pm 0.02)$ Å) which was obtained from a set of 6 independent experiments.

Disregarding experimental complications and contributions from adjacent spins, dipolar couplings extracted from build-up curves can be translated into distances using equation 7 only if anisotropic J-coupling, relaxation and chemical shift can be neglected and if the two-spin approximation holds. While simulations have helped to estimate errors introduced by the latter two factors, the systematic error introduced by relaxation and anisotropic J-coupling is difficult to quantify. For the systems which were investigated in this study only minor differences between the x-ray distance

and NMR distance were observed, indicating that the overall systematic error is small.

5 Conclusions

The results given in this paper may be summarized as follows: (i) Distance determination in relatively dense spin systems for example inorganic phosphates/biochemical systems is still possible if DQ constant time procedures are used, (ii) chemical shift compensation adapted to inorganic phosphates (big chemical shift anisotropy, small isotropic chemical shift difference) may be achieved by the use of supercycled symmetry-based sequences, namely $C7_1^3$ and $C9_1^4$. Simulations and measurements of phase and amplitude transients show that the design of DQ sequences needs to respect the restrictions imposed by transients.

Applications of constant-time DQ NMR to both organic and inorganic systems can be expected to help providing more accurate structural constraints. Applications of the presented techniques to amorphous C_3O_2 and PN are under way.

6 Acknowledgments

For preparation and characterization of the crystalline $Cd_2P_2S_6$ I would like to thank Felix Rheinauer and Robert Glaum. Support of SFB408 by the Deutsche Forschungsgemeinschaft is gratefully acknowledged. Moreover I would like to thank Mads Bak, Niels C. Nielsen, Thomas Vosegaard for the publication and maintenance of SIMPSON and Malcolm H. Levitt and Andreas Brinkmann for the C- and R-symmetry script. I am grateful to Wilfried Hoffbauer, Hellmut Eckert, Malcolm H. Levitt and his group for many inspiring talks. I would also like to thank Bernhard Klöckner for help with the acquisition of pulse transients and P. K. Madhu for commenting on the manuscript.

References

[1] D. D. Laws, H. M. L. Bitter, and A. Jerschow, Solid-state NMR spectroscopic methods in chemistry, *Angew. Chem., Int. Ed.* **41**, 3096–3129 (2002).

[2] R. Tycko, Biomolecular solid state NMR: Advances in structural methodology and applications to peptide and protein fibrils, *Annu. Rev. Phys. Chem.* **52**, 575–606 (2001).

[3] S. Dusold and A. Sebald, Dipolar recoupling under magic-angle spinning conditions, *Annu. rep. NMR Spectrosc.* **41**, 185–264 (2000).

[4] M. Baldus, Correlation experiments for assignment and structure elucidation of immobilized polypeptides under magic angle spinning, *Prog. Nucl. Magn. Reson. Spectrosc.* **41**, 1–47 (2002).

[5] S. P. Brown and H. W. Spiess, Advanced solid-state NMR methods for elucidation of structure and dynamics of molecular, macromolecular, and supramolecular systems, *Chem. Rev.* **101**, 4125–4155 (2001).

[6] A. E. Bennett, J. H. Ok, R. G. Griffin, and S. Vega, Chemical shift correlation spectroscopy in rotating solids: Radio frequency-driven dipolar recoupling and longitudinal exchange, *J. Chem. Phys.* **96**, 8624–8627 (1992).

[7] D. P. Raleigh, M. H. Levitt, and R. G. Griffin, Rotational Resonance in solid state NMR, *Chem. Phys. Letters* **146**, 71–76 (1988).

[8] Z. H. Gan and D. M. Grant, Pseudo-spin rotational resonance and homonuclear dipolar NMR of rotating solids, *Mol. Phys.* **67**, 1419–1430 (1989).

[9] N. C. Nielsen, H. Bildsoe, H. J. Jakobsen, and M. H. Levitt, Double-quantum homonuclear rotary resonance: efficient dipolar recovery in magic angle spinning nuclear magnetic resonance, *J. Chem. Phys.* **101**, 1805–1812 (1994).

[10] M. Feike, D. E. Demco, R. Graf, J. Gottwald, S. Hafner, and H. W. Spiess, Broadband multiple-quantum NMR spectroscopy, *J. Magn. Reson.* **A122**, 214–221 (1996).

[11] Y. K. Lee, N. D. Kurur, M. Helmle, O. G. Johannessen, N. C. Nielsen, and M. H. Levitt, Efficient dipolar recoupling in the NMR of rotating solids. A sevenfold symmetric radiofrequency pulse sequence, *Chem. Phys. Letters* **242**, 304–309 (1995).

[12] M. Carravetta, M. Edén, X. Zhao, A. Brinkmann, and M. H. Levitt, Symmetry principles for the design of radiofrequency pulse sequences in the nuclear magnetic resonance of rotating solids, *Chem. Phys. Letters* **321**, 205–215 (2000).

[13] M. Baldus and B. H. Meier, Broadband polarization transfer under magic-angle spinning: application to total through-space-correlation NMR spectroscopy, *J. Magn. Reson.* **128**, 172–193 (1997).

[14] R. Tycko and G. Dabbagh, Double-quantum filtering in magic-angle-spinning NMR spectroscopy: An appraoch to spectral simplification and molecular structure determination, *J. Am. Chem. Soc.* **113**, 9444–9448 (1991).

[15] D. M. Gregory, G. M. Wolfe, T. P. Jarvie, J. C. Shiels, and G. P. Drobny, Double-quantum filtering in magic-angle-spinning NMR spectroscopy applied to DNA oligomers, *Mol. Phys.* **89**, 1835–1849 (1996).

[16] M. Munowitz, A. Pines, and M. Mehring, Multiple-quantum dynamics in NMR: A directed walk through Liouville space, *Journal of Chemical Physics* **86**, 3172–3182 (1987).

[17] J. Schmedt auf der Günne and H. Eckert, High-resolution double-quantum ^{31}P NMR: A new approach to structural studies of thiophosphates, *Chem. Eur. J.* **4**, 1762–1767 (1998).

[18] J. Schmedt auf der Günne, S. Kaczmarek, L. van Wüllen, H. Eckert, D. Paschke, A. J. Foecker, and W. Jeitschko, Solid state NMR connectivity studies in dipolarly coupled inorganic networks: Crystal structure and site assignments for the lithium phosphide LiP_5, *J. Solid State Chem.* **147**, 341–349 (1999).

[19] W. A. Dollase, M. Feike, H. Förster, T. Schaller, I. Schnell, A. Sebald, and S. Steuernagel, A 2D ^{31}P MAS NMR study of polycrystalline $Cd_3(PO_4)_2$, *J. Am. Chem. Soc.* **119**, 3807–3810 (1997).

[20] S. Kiihne, K. B. Geahigan, N. A. Oyler, H. Zebroski, M. A. Mehta, and G. P. Drobny, Distance measurements in multiply labeled crystalline cytidines by dipolar recoupling solid state NMR, *J. Phys. Chem.* **A103**, 3890–3903 (1999).

[21] S. Kiihne, A. Metha, J. A. Stringer, D. M. Gregory, J. C. Shiels, and G. P. Drobny, Distance measurements by dipolar recoupling two-dimensional sold-state NMR, *J. Phys. Chem.* **102**, 2274–2282 (1998).

[22] M. Carravetta, M. Edén, O. G. Johannessen, H. Luthman, P. J. E. Verdegem, J. Lugtenburg, A. Sebald, and M. H. Levitt, Estimation of carbon-carbon bond lengths and medium-range internuclear: Distances by solid-state nuclear magnetic resonance, *J. Am. Chem. Soc.* **123**, 10628–10638 (2001).

[23] A. E. Bennett, D. P. Weliky, and R. Tycko, Quantitative conformational measurements in solid state NMR by constant-time homonuclear dipolar recoupling, *J. Am. Chem. Soc.* **120**, 4897–4898 (1998).

[24] Y. Ishii, ^{13}C-^{13}C dipolar recoupling under very fast magic angle spinning in solid-state nuclear magnetic resonance: Applications to distance measurements, spectral assignments, and high-throughput secondary-structure determination, *J. Chem. Phys.* **114**, 8473–8483 (2001).

[25] P. E. Kristiansen, D. J. Mitchell, and J. N. S. Evans, Double-quantum dipolar recoupling at high magic-angle spinning rates, *J. Magn. Reson.* **157**, 253–266 (2002).

[26] P. Toffoli, P. Khodadad, and N. Rodier, Structure du tétrathiomonophosphate(V) Heptathiodiphosphate(V) d'Argent, *Acta Cryst.* **B38**, 2374–2378 (1982).

[27] K. Y. Leung and C. Calvo, The structure of $Na_4P_2O_7$ at 22 °C, *Can. J. Chem.* **50**, 2519–2526 (1972).

[28] G. Ouvard, R. Brec, and J. Rouxel, Structural determination of some MPS_3 layered phases (M = Mn, Fe, Co, Ni and Cd), *Mater. Res. Bull.* **20**, 1181–1189 (1985).

[29] P.-G. Jönsson and Å. Kvick, Precision neutron diffraction structure determination of protein and nucleic acid components. III. The crystal and molecular structure of the amino acid α-glycine, *Acta Cryst.* **B28**, 1827–1833 (1972).

[30] Z. Zhang, J. H. Kennedy, and H. Eckert, Glass formation and structure in Non-oxide chalcogenide systems. the short range order of Ag_2S-P_2S_5 glasses, *J. Am. Chem. Soc.* **114**, 5775–5784 (1992).

[31] L. Griffiths, A. Root, R. K. Harris, and K. J. Parker, Magic-angle spinning phosphorus-31 nuclear magnetic resonance of polycrystalline sodium phosphates, *J. Chem. Soc. Dalton Trans.* 2247–2251 (1986).

[32] S. Hayashi and K. Hayamizu, High-resolution solid-state ^{31}P NMR of alkali phosphates, *Bull. Chem. Soc. Jpn.* **62**, 3061–3068 (1989).

[33] J. Schmedt auf der Günne, H. Eckert, A. Léaustic, and F. Babonneau, Vacancy ordering and host-guest interactions in $CdPS_3$ intercalates: Results from multidimensional solid state NMR, *Phys. Chem. Chem. Phys.* **5**, 1306–1313 (2003).

[34] R. R. Ernst, G. Bodenhausen, and A. Wokaun, *Principles of nuclear magnetic resonance in one and two dimensions*, International Series of Monographs on Chemistry, Oxford University Press (1987).

[35] M. H. Levitt, P. K. Madhu, and C. E. Hughes, Cogwheel phase cycling, *J. Magn. Reson.* **155**, 300–306 (2002).

[36] G. Metz, X. Wu, and S. O. Smith, Ramped-amplitude cross polarization in magic-angle-spinning NMR, *J. Magn. Reson.* **A 110**, 219–227 (1994).

[37] M. Hohwy, H. J. Jakobsen, M. Edén, M. H. Levitt, and N. C. Nielsen, Broadband dipolar recoupling in the nuclear magnetic resonance of rotating solids: A compensated C7 pulse sequence, *J. Chem. Phys.* **108**, 2686–2694 (1998).

[38] M. Bak, J. T. Rasmussen, and N. C. Nielsen, SIMPSON: A general simulation program for solid-state NMR spectroscopy, *J. Magn. Reson.* **147**, 296–330 (2000).

[39] H. Conroy, Molecular Schrödinger equation. VIII. A new method for the evaluation of multi-dimensional integrals, *J. Chem. Phys.* **47**, 5307–5318 (1967).

[40] SIMPSON is offering now an implementation (C-MINUIT) of the CERN-MINUIT tools for function minimization. MINUIT is part of the CERN program library .

[41] S. Wolfram, *Mathematica: A system for doing mathematics by computer*, Addison-Wesley, New York (1991).

[42] M. H. Levitt, The signs of frequencies and phases in NMR, *J. Magn. Reson.* **126**, 164–182 (1997).

[43] R. A. Haberkorn, R. E. Stark, H. van Willigen, and R. G. Griffin, Determination of bond distances and bond angles by solid-state nuclear magnetic resonance. ^{13}C and ^{14}N NMR study of glycine, *J. Am. Chem. Soc.* **103**, 2534–2539 (1981).

[44] A. Kubo and C. A. McDowell, One- and two-dimensional ^{31}P cross-polarization magic-angle-spinning nuclear magnetic resonance studies on two-spin systems with homonuclear dipolar coupling and J coupling, *Journal of Chemical Physics* **92**, 7156–7170 (1990).

[45] M. H. Levitt, Symmetry-based pulse sequence in magic-angle spinning solid-state NMR, *Encyclopedia of NMR* **9**, 165–196 (2002).

[46] A. Brinkmann and M. H. Levitt, Symmetry principles in the nuclear magnetic resonance of spinning solids: Heteronuclear recoupling by generalized Hartmann-Hahn sequences, *Journal of Chemical Physics* **115**, 357–384 (2001).

[47] M. Hohwy, C. M. Rienstra, C. P. Jaroniec, and R. G. Griffin, Fivefold symmetric homonuclear dipolar recoupling in rotating solids: Application to double quantum spectroscopy, *J. Chem. Phys.* **110**, 7983–7992 (1999).

[48] R. Graf, D. E. Demco, J. Gottwald, S. Hafner, and H. W. Spiess, Dipolar couplings and internuclear distances by double-quantum nuclear magnetic resonance, *J. Chem. Phys.* **106**, 885–895 (1997).

[49] S. M. De Paul, K. Saalwächter, R. Graf, and H. W. Spiess, Sideband patterns from rotor-encoded longitudinal magnetization in MAS recoupling experiments, *J. Magn. Reson.* **146**, 140–156 (2000).

[50] A. Brinkmann, M. Edén, and M. H. Levitt, Synchronous helical pulse sequences in magic-angle spinning nuclear magnetic resonance:Double quantum recoupling of multiple-spin systems, *J. Chem. Phys.* **112**, 8539–8554 (2000).

[51] A. Brinkmann, J. Schmedt auf der Günne, and M. H. Levitt, Homonuclear zero-quantum recoupling in fast magic-angle spinning nuclear magnetic resonance, *J. Magn. Reson.* **156**, 79–96 (2002).

List of Figures

Table 1: Chemical shift parameters and longitudinal relaxation time constants T_1 for the crystalline phosphates used. Chemical shift parameters were obtained by fitting the experimental spectrum with simulated spectra in single spin approximation, i.e. neglecting the dipolar interaction. Exception: † Simulated spectra were calculated for a two spin system including the chemical shift, magnetic dipole dipole interaction and a center of inversion.

compound	δ_{iso}/ppm	δ_{aniso}/ppm	η	$r/10^{-2}$	crystal structure	$T_1(T = 20.0\,^{\circ}\mathrm{C})/s$
$Ag_7P_3S_{11}$	103.2	-15	0.54	4.2	[26]	32
	101.4	-50	0.42			27
	92.0	$+40$	0.74			32
$Cd_2P_2S_6$†	103.4	$+18$	0.88	3.5	[28]	> 2200
$Na_4P_2O_7$	2.7	$+88$	0.26	3.6	[27]	195

Table 2: Candidate C-/R-Symmetries suitable for γ-encoded dipolar DQ excitation; listed are the best 32 supercycled C-/R-pulse sequences sorted by their chemical shift compensation which is reflected in the parameter B_{max}; in the column with the C- and R-elements the composite pulse is given in the notation $flipangle_{pulse\,phase}$ in degrees; the column "Type" refers to the recoupled average Hamiltonian $\bar{\mathcal{H}}^{(1)}_{lm\lambda\mu}$, "A" denotes terms with (l,m,λ,μ) equal $(2,-1,2,2)$,$(2,1,2,-2)$ and "B" denotes terms with (l,m,λ,μ) equal $(2,1,2,2)$,$(2,-1,2,-2)$; more details can be found in the text.

C-Class						R-Class					
CN^{ν}_{n}	Type	C-Element	B_{max}/T	$\lvert\kappa\rvert$	$\frac{\nu_{rf}}{\nu_{mas}}$	RN^{ν}_{n}	Type	R-Element	B_{max}	$\lvert\kappa\rvert$	$\frac{\nu_{rf}}{\nu_{mas}}$
$C17^{8}_{1}$	A	$90_0-360_{180}-270_0$	12.9	0.1758	34	$R32^{31}_{2}$	A	180_0	13.9	0.1763	8
$C15^{7}_{1}$	A	$90_0-360_{180}-270_0$	12.8	0.1755	30	$R34^{33}_{2}$	A	180_0	13.7	0.1764	8.5
$C13^{6}_{1}$	A	$90_0-360_{180}-270_0$	12.5	0.1751	26	$R36^{35}_{2}$	A	180_0	12.8	0.1764	9
$C11^{5}_{1}$	A	$90_0-360_{180}-270_0$	12.1	0.1745	22	$R38^{37}_{2}$	A	180_0	12.6	0.1765	9.5
$C9^{4}_{1}$	A	$90_0-360_{180}-270_0$	11.3	0.1733	18	$R40^{39}_{2}$	A	180_0	12.4	0.1765	10
$C16^{7}_{2}$	A	$90_0-360_{180}-270_0$	10.6	0.1724	16	$R30^{14}_{2}$	A	$60_0-300_{180}-60_0$	11.4	0.1343	17.5
$C7^{3}_{1}$	A	$90_0-360_{180}-270_0$	9.3	0.1711	14	$R20^{9}_{2}$	A	$60_0-300_{180}-60_0$	11.3	0.1334	11.66
$C18^{1}_{2}$	B	$90_0-360_{180}-270_0$	8.7	0.1733	18	$R24^{11}_{2}$	A	$60_0-300_{180}-60_0$	11.2	0.1339	14
$C17^{1}_{2}$	B	$90_0-360_{180}-270_0$	8.5	0.1729	17	$R28^{13}_{2}$	A	$60_0-300_{180}-60_0$	11.2	0.1342	16.34
$C16^{1}_{2}$	B	$90_0-360_{180}-270_0$	8.3	0.1724	16	$R16^{7}_{2}$	A	$60_0-300_{180}-60_0$	11.1	0.1325	9.34
$C15^{1}_{2}$	B	$90_0-360_{180}-270_0$	8.0	0.1718	15	$R26^{12}_{2}$	A	$60_0-300_{180}-60_0$	11.1	0.1341	15.16
$C20^{1}_{2}$	B	360_0	7.9	0.1743	10	$R22^{10}_{2}$	A	$60_0-300_{180}-60_0$	11.0	0.1337	12.84
$C14^{1}_{2}$	B	$90_0-360_{180}-270_0$	7.8	0.1711	14	$R18^{8}_{2}$	A	$60_0-300_{180}-60_0$	10.7	0.1330	10.5
$C19^{9}_{1}$	A	360_0	7.6	0.1761	19	$R12^{5}_{2}$	A	$60_0-300_{180}-60_0$	10.5	0.1306	7
$C17^{8}_{1}$	A	360_0	7.6	0.1759	17	$R30^{13}_{4}$	A	$60_0-300_{180}-60_0$	10.3	0.1321	8.76
$C15^{7}_{1}$	A	360_0	7.5	0.1757	15	$R30^{28}_{4}$	A	90_0-270_{180}	10.3	0.1724	7.5
$C13^{1}_{2}$	B	$90_0-360_{180}-270_0$	7.5	0.1702	13	$R14^{6}_{2}$	A	$60_0-300_{180}-60_0$	10.1	0.1318	8.16
$C19^{1}_{2}$	B	360_0	7.4	0.1741	9.5	$R26^{11}_{4}$	A	$60_0-300_{180}-60_0$	9.6	0.1312	7.58
$C13^{6}_{1}$	A	360_0	7.4	0.1753	13	$R34^{32}_{4}$	A	90_0-270_{180}	9.3	0.1734	8.5
$C12^{1}_{2}$	B	$90_0-360_{180}-270_0$	7.2	0.1691	12	$R14^{13}_{2}$	A	90_0-270_{180}	9.2	0.1718	7
$C11^{5}_{1}$	A	360_0	7.1	0.1747	11	$R28^{26}_{4}$	A	90_0-270_{180}	9.2	0.1718	7
$C18^{1}_{2}$	B	360_0	7.0	0.1737	9	$R36^{34}_{4}$	A	90_0-270_{180}	9.2	0.1737	9
$C20^{9}_{2}$	A	360_0	6.9	0.1743	10	$R18^{17}_{2}$	A	90_0-270_{180}	9.2	0.1737	9
$C11^{1}_{2}$	B	$90_0-360_{180}-270_0$	6.8	0.1677	11	$R36^{17}_{2}$	A	90_0-270_{180}	9.0	0.1760	18
$C17^{1}_{2}$	B	360_0	6.6	0.1734	8.5	$R30^{28}_{4}$	A	$60_0-300_{180}-60_0$	8.9	0.1322	8.76
$C10^{1}_{2}$	B	$90_0-360_{180}-270_0$	6.5	0.1658	10	$R16^{15}_{2}$	A	$60_0-300_{180}-60_0$	8.9	0.1325	9.34
$C9^{4}_{1}$	A	360_0	6.5	0.1737	9	$R24^{22}_{4}$	A	$60_0-300_{180}-60_0$	8.9	0.1306	7
$C12^{5}_{2}$	A	$90_0-360_{180}-270_0$	6.4	0.1691	12	$R12^{11}_{2}$	A	$60_0-300_{180}-60_0$	8.9	0.1306	7
$C16^{1}_{2}$	B	360_0	6.3	0.1729	8	$R34^{16}_{2}$	A	90_0-270_{180}	8.8	0.1759	17
$C9^{1}_{2}$	B	$90_0-360_{180}-270_0$	6.1	0.1633	9	$R22^{21}_{2}$	A	90_0-270_{180}	8.8	0.1747	11
$C16^{7}_{2}$	A	360_0	6.1	0.1729	8	$R20^{19}_{2}$	A	90_0-270_{180}	8.8	0.1743	10
$C15^{1}_{2}$	B	360_0	6.0	0.1724	7.5	$R32^{15}_{2}$	A	90_0-270_{180}	8.7	0.1758	16

Table 3: Internuclear ^{31}P-^{31}P distances for $Ag_7P_3S_{11}$, $Na_4P_2O_7$, $Cd_2P_2S_6$ and the ^{13}C-^{13}C distances for glycine taken from single-crystal X-ray structures; Given are internuclear distances d_1 for the excited DQ coherences and the distance to the next nearest neighbor d_2

	$d_1/\text{Å}$	$d_2/\text{Å}$	$\frac{d_2}{d_1}$
$Ag_7P_3S_{11}$	3.564	5.010	1.41
$Na_4P_2O_7$	2.936	4.762	1.62
$Cd_2P_2S_6$	2.223	4.786	2.15
glycine	1.526	3.104	2.03

Table 4: Comparison of internuclear ^{31}P-^{31}P distances d for $Ag_7P_3S_{11}$, $Na_4P_2O_7$, $Cd_2P_2S_6$ and the ^{13}C-^{13}C distances for glycine as measured by X-ray diffraction and NMR; compare Fig. 9,10, 11 and 12

	X-ray	NMR
	$d/$Å	d(DQ-CT)/Å
$Ag_7P_3S_{11}$	3.564	3.32
$Na_4P_2O_7$	2.936	2.94
$Cd_2P_2S_6$	2.223	2.33
glycine	1.526	1.53

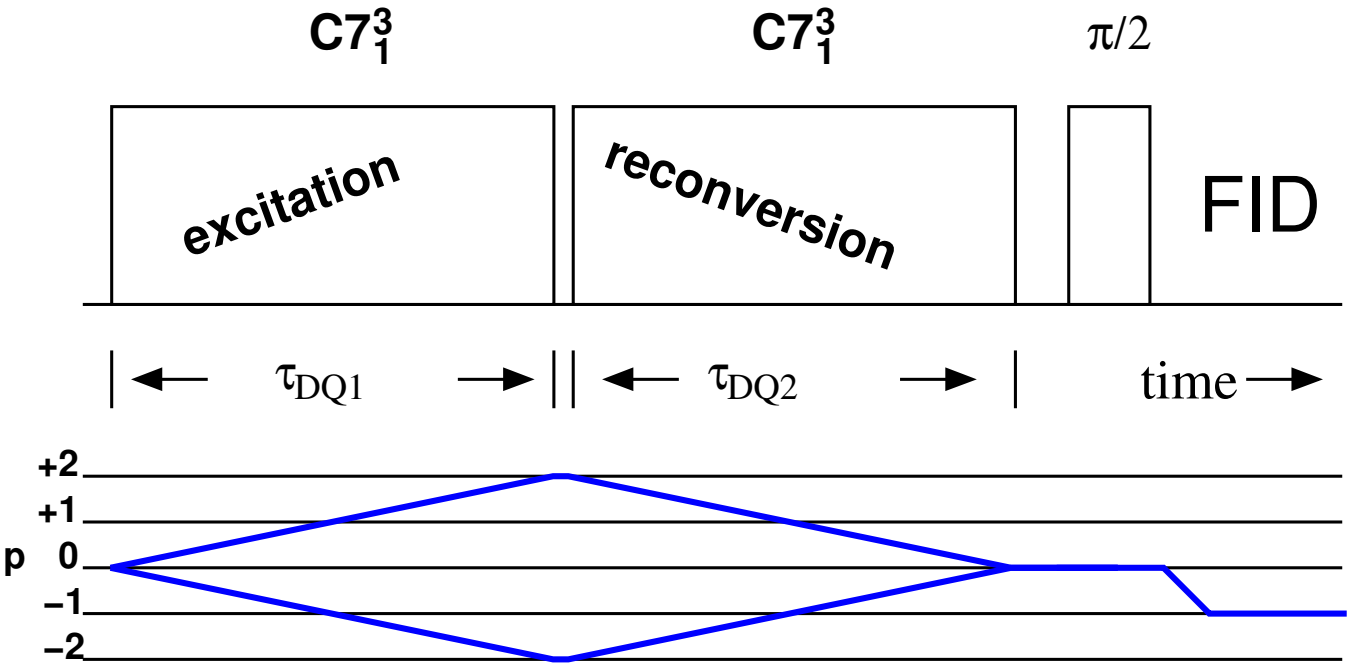

Figure 1: DQ pulse sequences (schematic); DQ-pulse sequence used for distance determination in symmetric, asymmetric and constant time excitation schemes (see text).

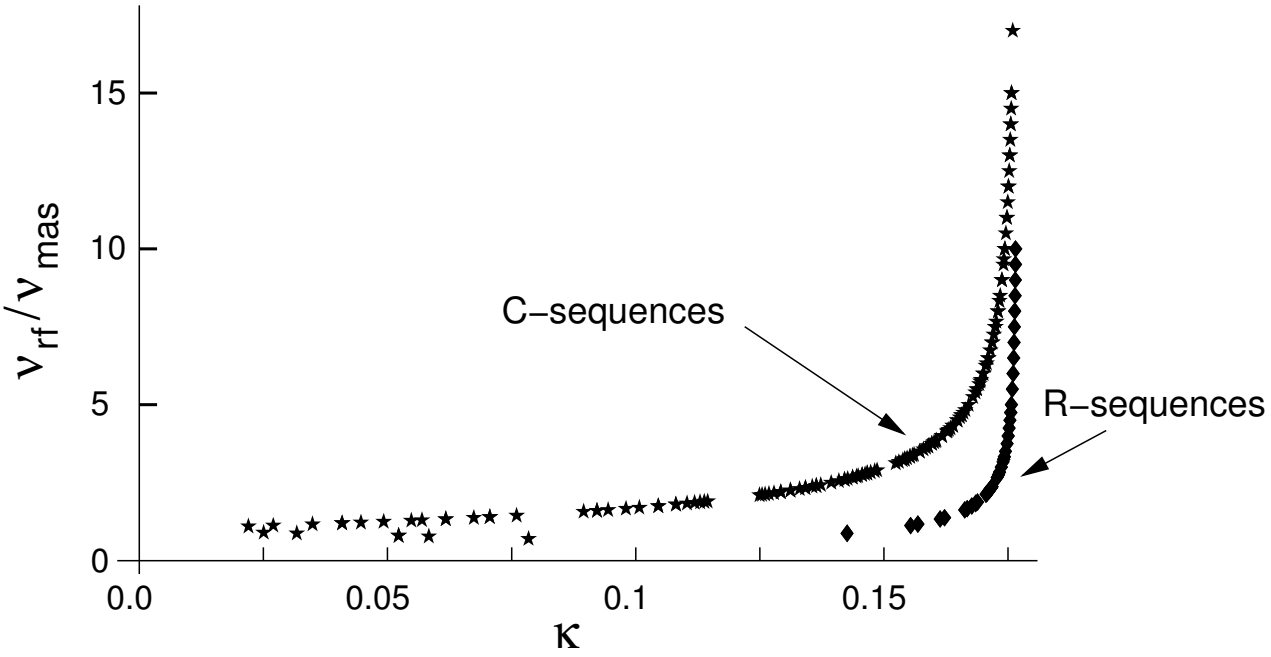

Figure 2: Scaling factor as a function of the rf-demand $\frac{\nu_{rf}}{\nu_r}$ for several C- and R-symmetries with the basic elements C=360_0 and R=180_0, respectively.

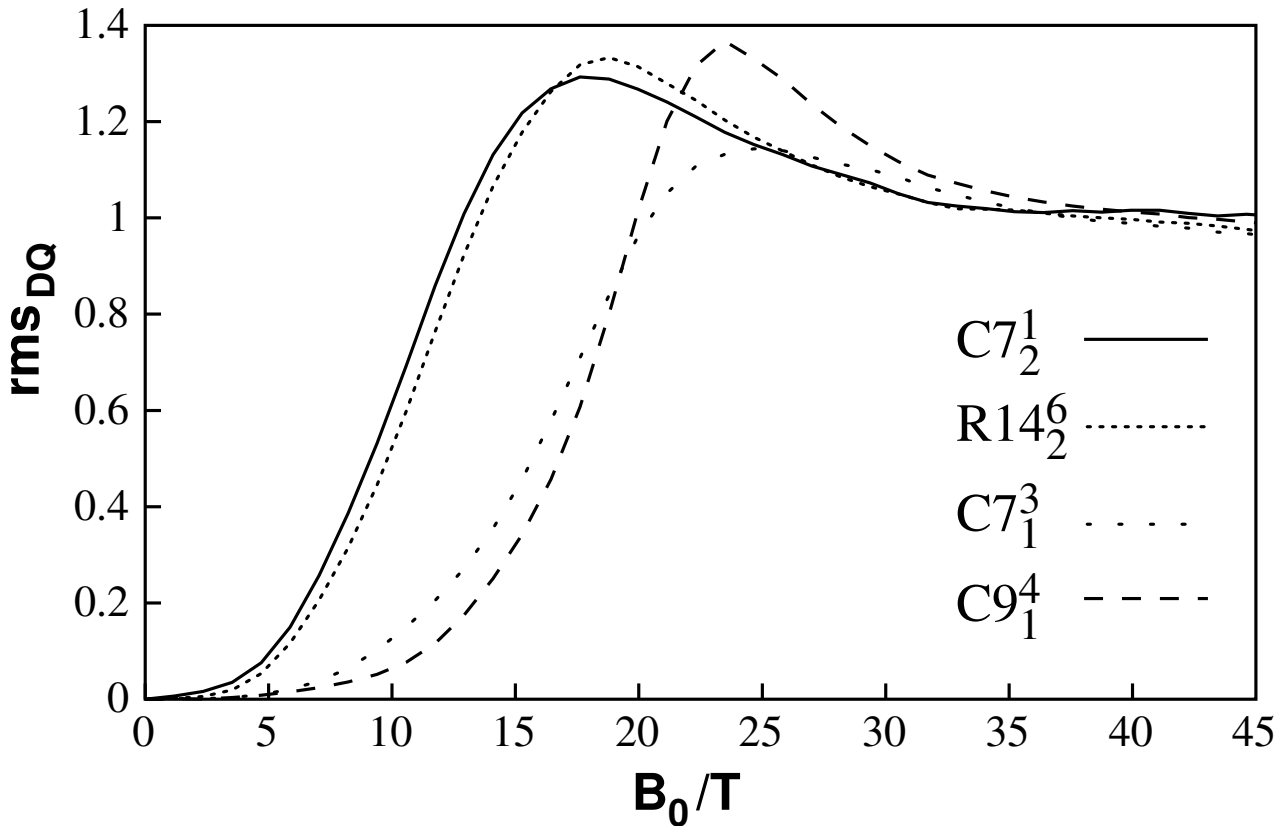

Figure 3: Deviation from the ideal DQ build-up curve rms_{DQ} as a function of the external magnetic field; individual DQ build-up curves were calculated for pulse sequences with the symmetries $R14^6_2$, $C7^1_2$, $C7^3_1$ and $C9^4_1$ using $90_0 - 360_{180} - 270_0$ as C-element and $90_0 - 270_{180}$ as R-element respectively and the spin-parameters of $Na_4P_2O_7$ as given in Tables 1 and 3 (simulation conditions: 2-spin approximation including dipolar interaction and chemical shift, rf nutation frequency used for DQ-excitation 70 kHz).

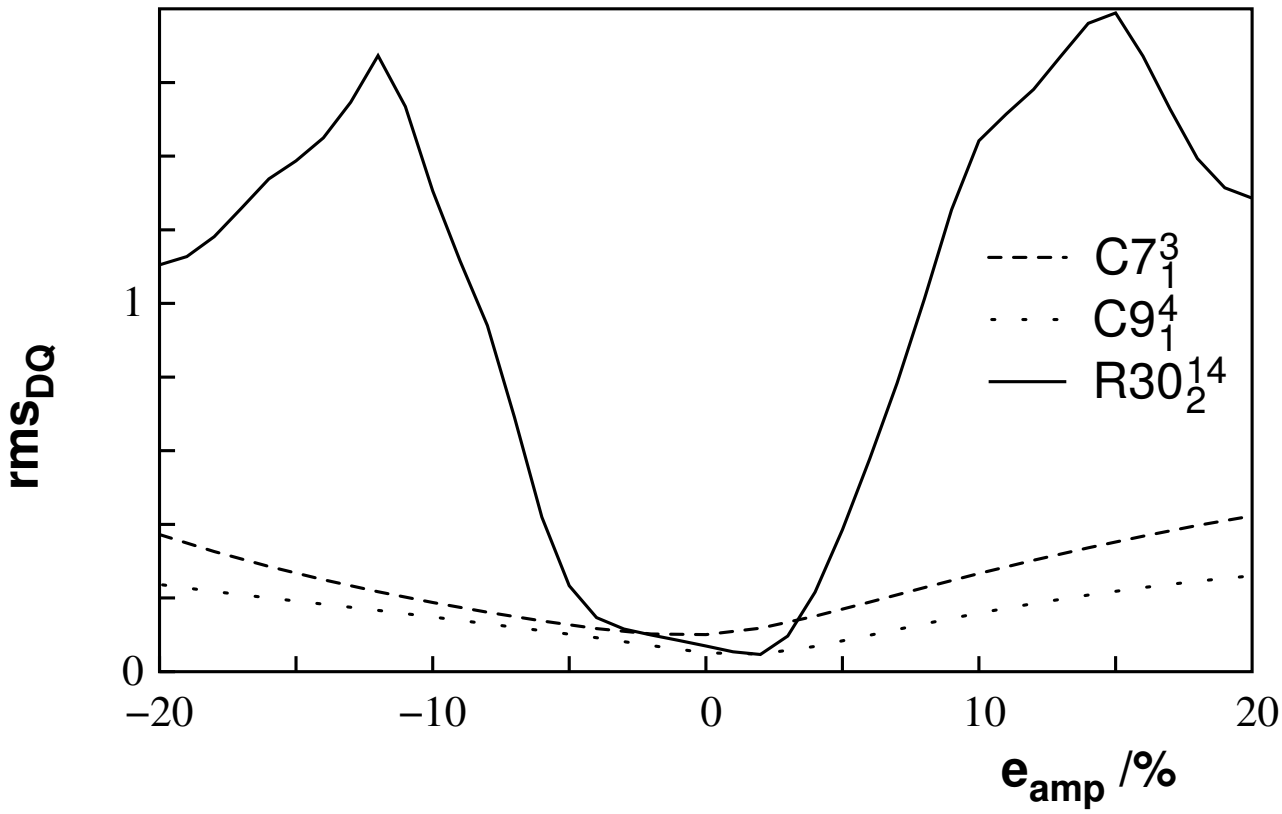

Figure 4: Deviation from the ideal DQ build-up curve as a function of the amplitude error for the pulse sequences $C7_1^3$, $C9_1^4$ and $R30_2^{14}$ with the elements C=$90_0 - 360_{180} - 270_0$ and R=$60_0 - 300_{180} - 60_0$ respectively.

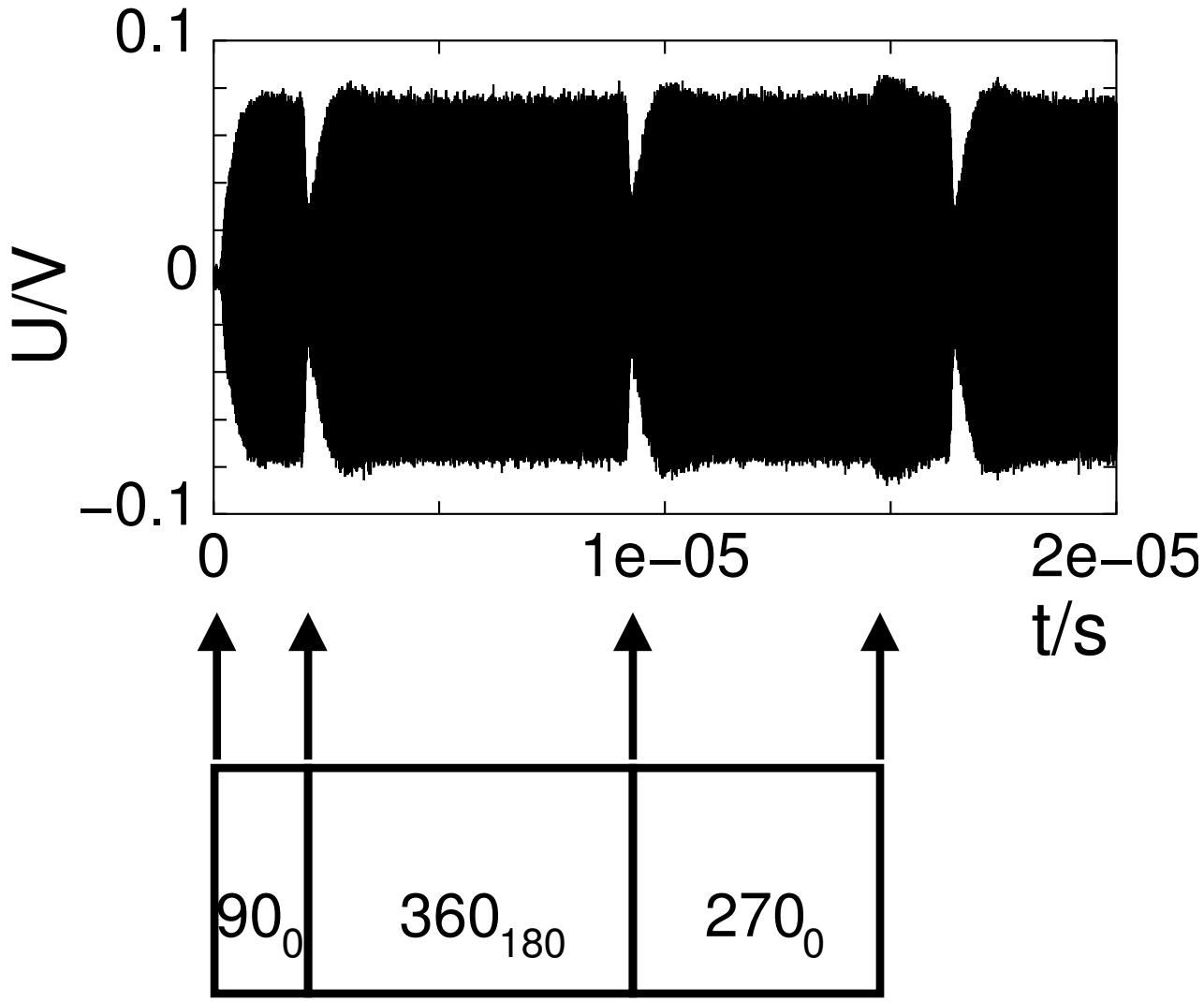

Figure 5: Pulse and phase transients monitored from the voltage in a pickup coil for a pulse train of $C7_2^1$ with an element C$= 90_0 - 360_{180} - 270_0$ at 20 kHz spinning speed.

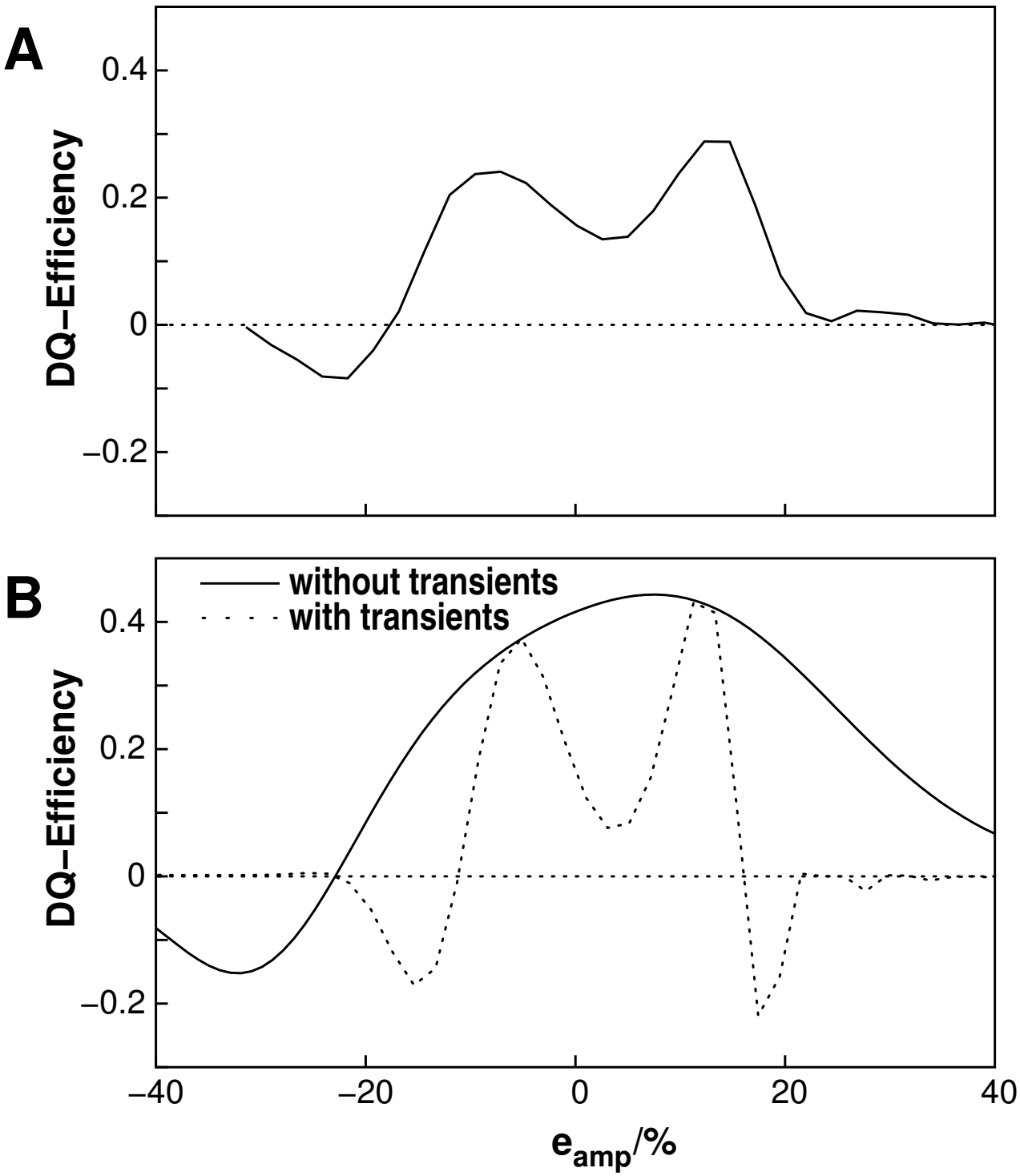

Figure 6: Influence of phase and amplitude transients: ^{31}P DQ efficiency as a function of the amplitude error e_{amp}; **A** experimental curve, **B** simulated curves with and without the influence of pulse and phase transients for the ^{31}P spin-pair in the heptathiodiphosphate group in crystalline $Ag_7P_3S_{11}$, using $C7_2^1$ with the C-element $90_0 - 360_{180} - 270_0$ at 10 kHz spinning frequency and $\tau_{DQ} = 1.6$ ms.

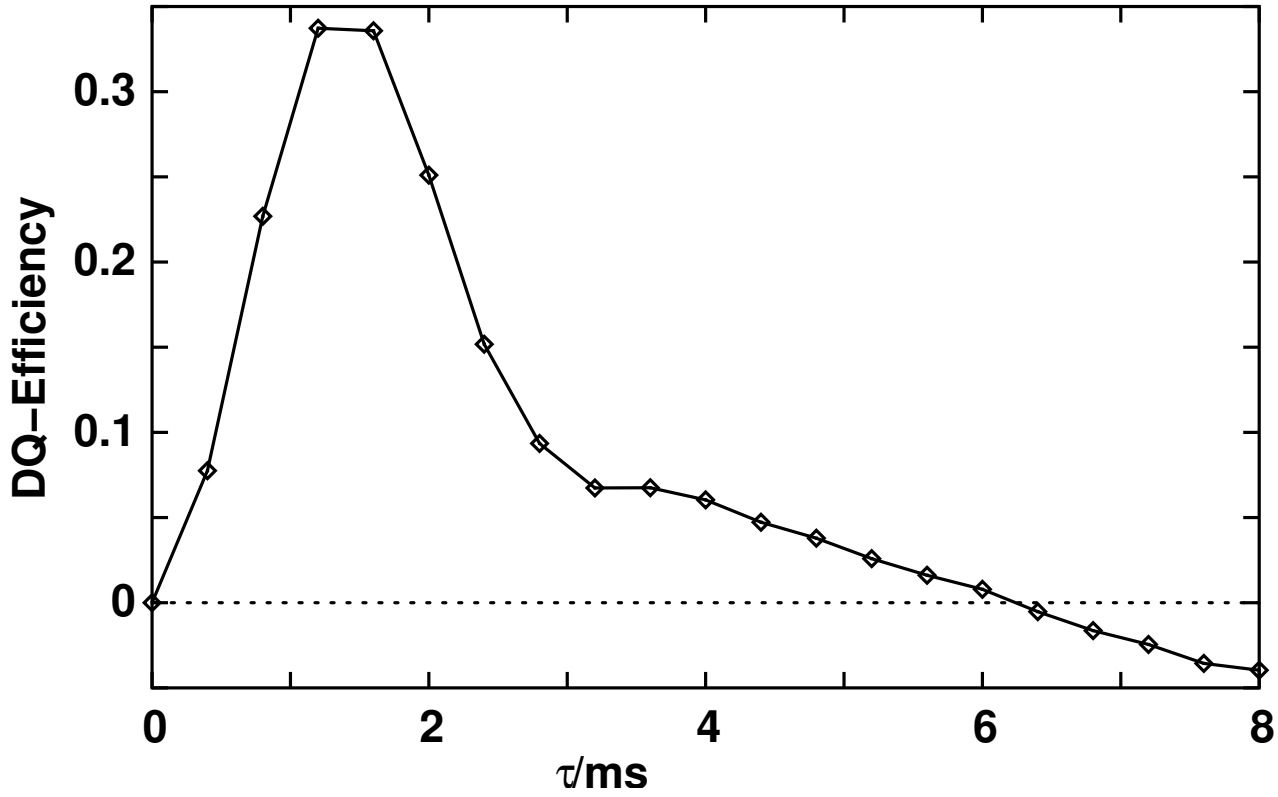

Figure 7: Experimental ^{31}P DQ build-up curve acquired according to the symmetric procedure for $Na_4P_2O_7$ using pulse sequence Fig. 1,$C7_1^3$, super cycling and the C-element $90_0 - 360_{180} - 270_0$, $\nu_r = 5\,\mathrm{kHz}$.

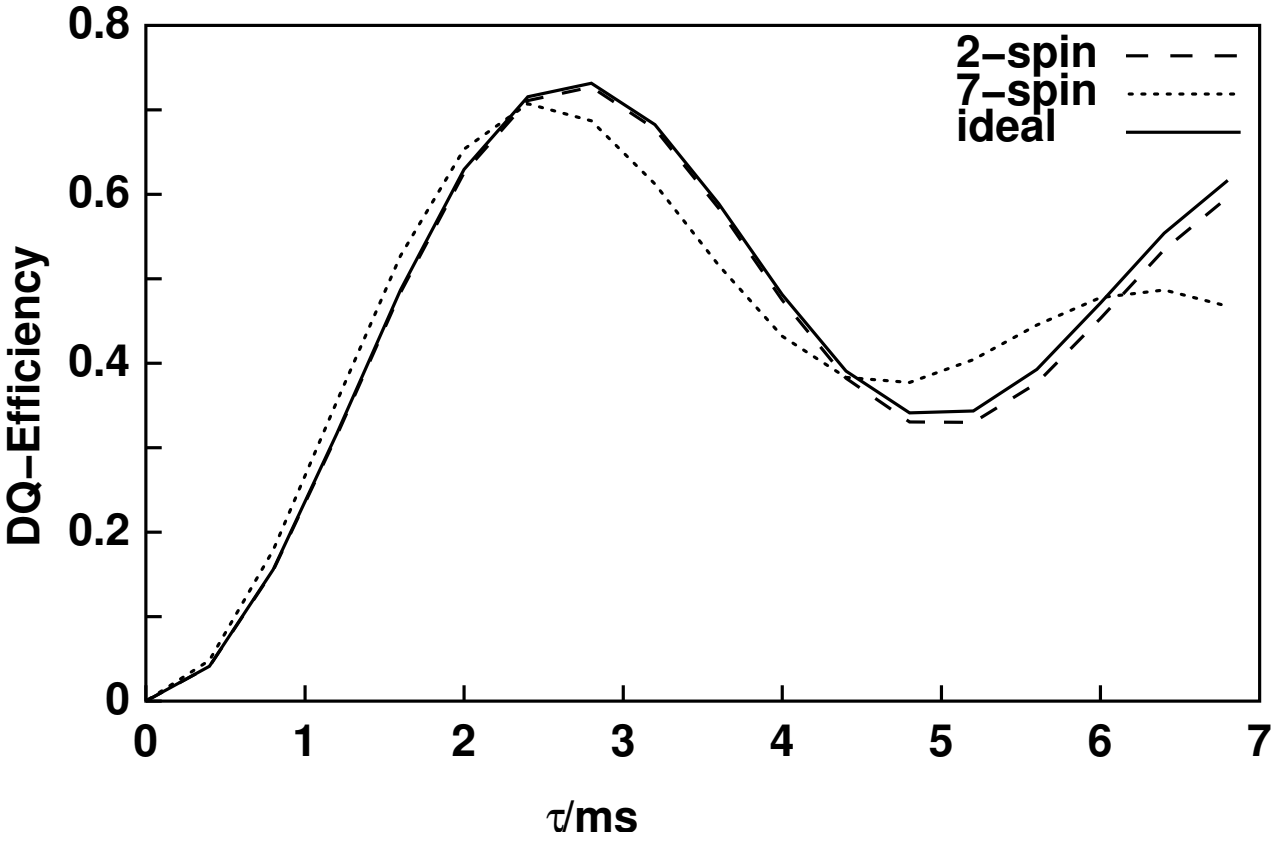

Figure 8: Influence of the size of the spin system onto the ^{31}P DQ build-up curve for the P_2S_7 group in crystalline $Ag_7P_3S_{11}$ using supercycled $C7_1^3$ with the C-element $90_0 - 360_{180} - 270_0$ at 5 kHz spinning frequency; shown are curves for 2-spin calculations without (denoted ideal) and with chemical shift interaction (denoted 2-spin) and for the DQ filtered intensities of the same two spins under the influence of 5 closest spins and the chemical shift (denoted 7-spin).

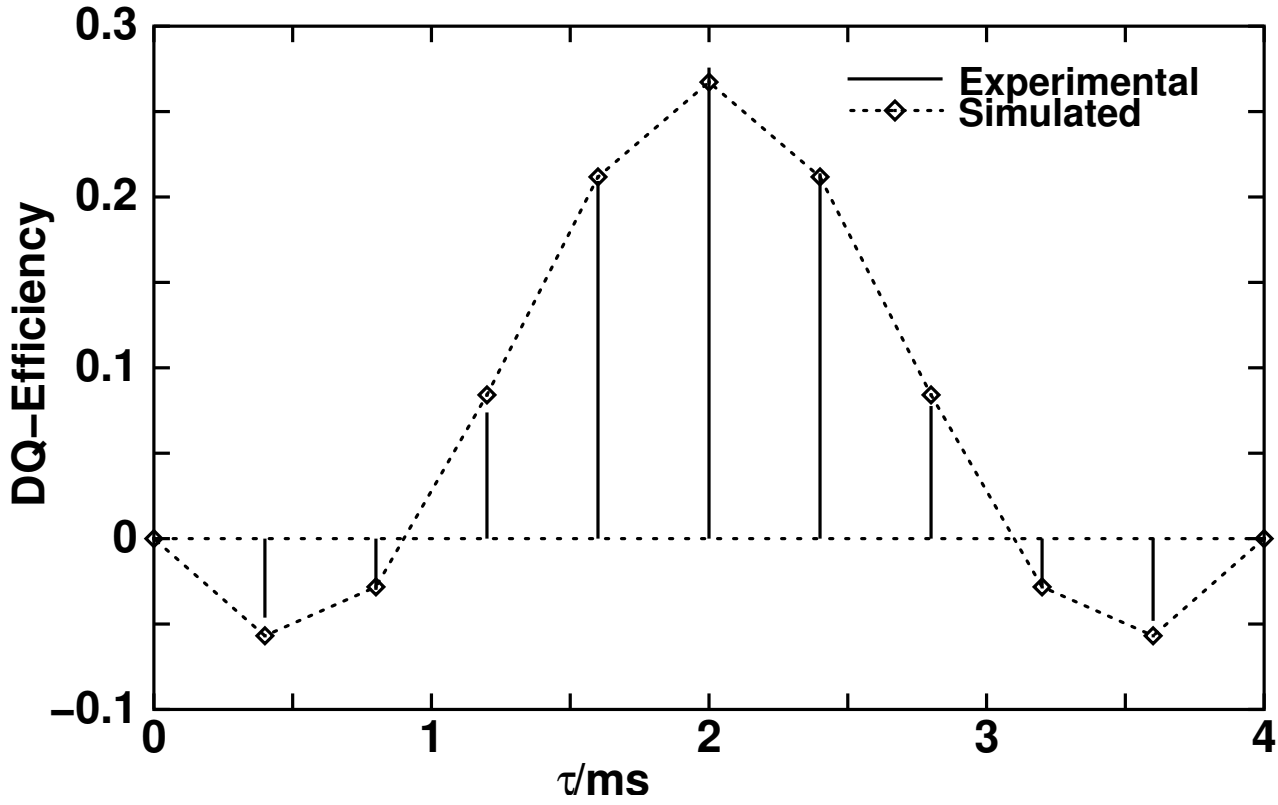

Figure 9: ^{31}P Constant-time DQ build-up curves for $Na_4P_2O_7$ using supercycled $C7_1^3$ with the C-element $90_0 - 360_{180} - 270_0$ at 5 kHz spinning frequency; vertical bars: experimental data; points with dotted lines: best fit corresponding to $\nu_{dip} = -774$ Hz and $r = 0.024$; lines are meant as guide to the eye.

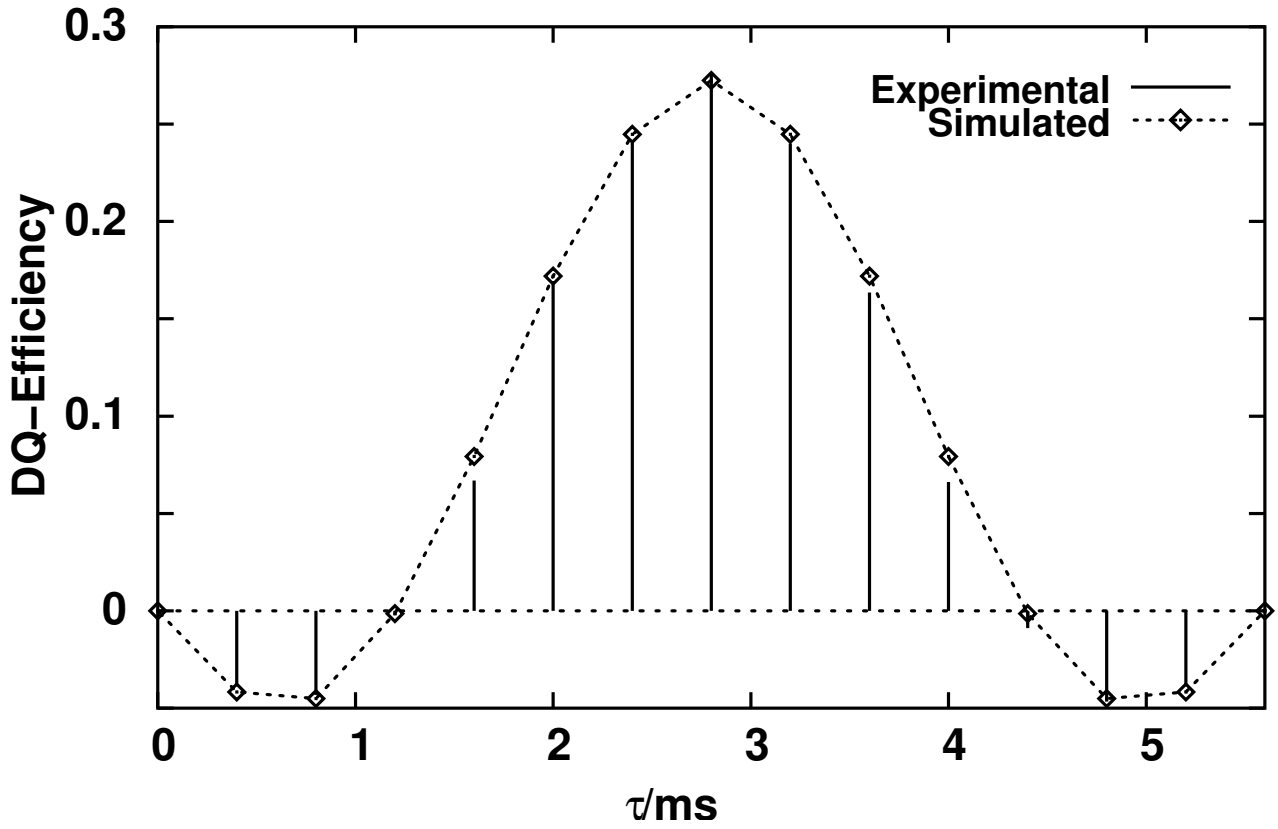

Figure 10: ^{31}P Constant-time DQ build-up curves for the P_2S_7-group in crystalline $Ag_7P_3S_{11}$ using supercycled $C7_1^3$ with the C-element $90_0 - 360_{180} - 270_0$ at 5 kHz spinning frequency, vertical bars: experimental data; points with dotted lines: best fit corresponding to $\nu_{dip} = -545$ Hz and $r = 0.017$; lines are meant as guide to the eye.

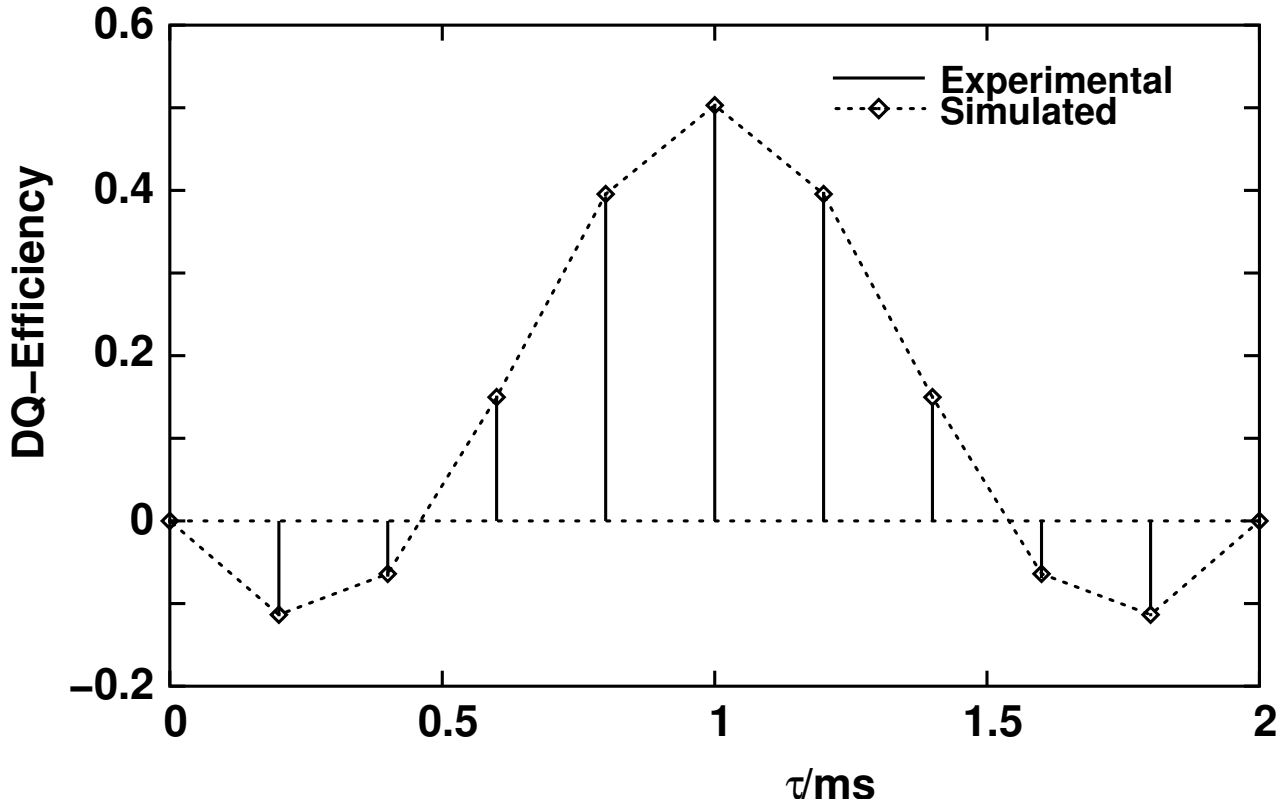

Figure 11: ^{31}P Constant-time DQ build-up curves for $Cd_2P_2S_6$ using supercycled $C7_1^3$ with the C-element $90_0 - 360_{180} - 270_0$ at 5 kHz spinning frequency, vertical bars: experimental data; points with dotted lines: best fit corresponding to $\nu_{Dip} = -1563$ Hz and $r = 0.007$; lines are meant as guide to the eye.

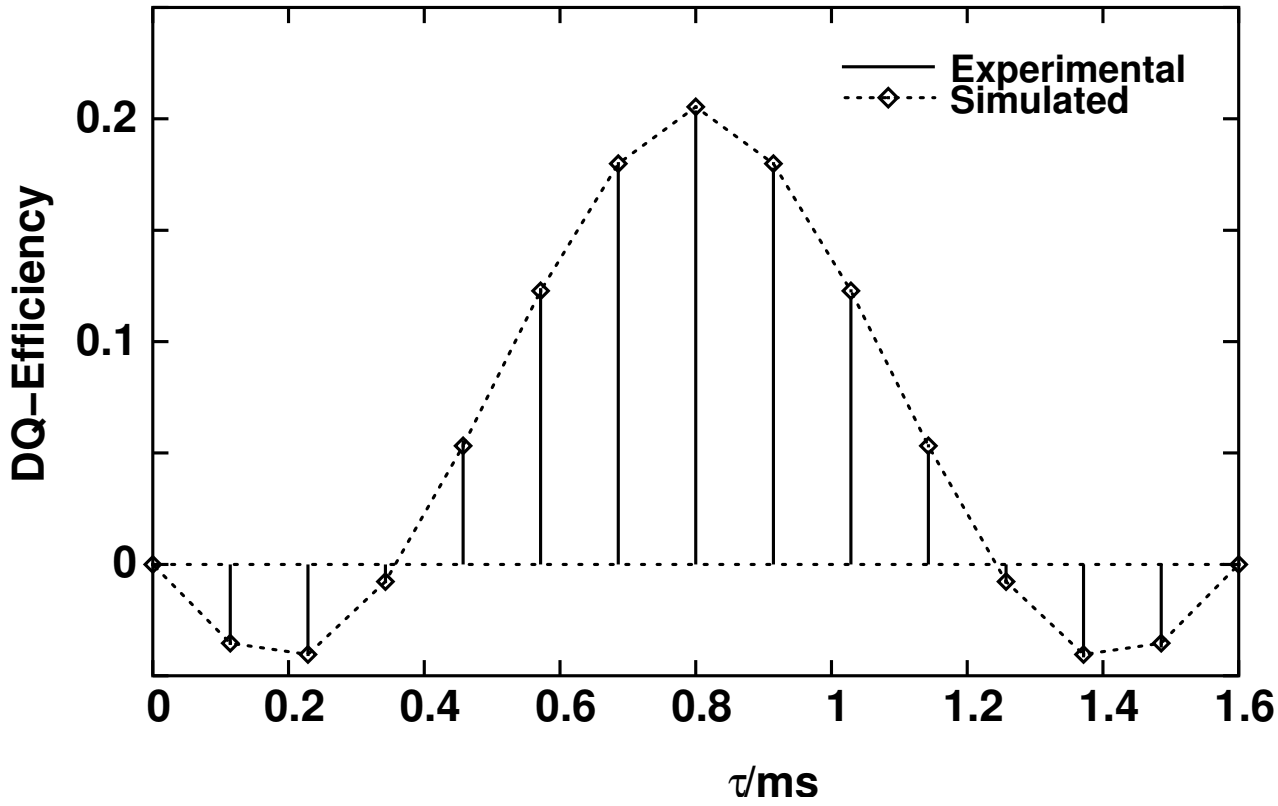

Figure 12: ^{13}C Constant-time DQ build-up curves for glycine $C7^1_2$, C-element $90_0 - 360_{180} - 270_0$, super cycle $\left[C7^1_2\right]_{+0^\circ}\left[C7^1_2\right]_{+180^\circ}$; vertical bars: experimental data; points with dotted lines (as guide to the eye): best fit corresponding to $\nu_{dip} = -2128\,\mathrm{Hz}$ and $r = 0.007$; lines are meant as guide to the eye; $\nu_r = 5\,\mathrm{kHz}$; DQ conversion times were incremented in steps of 2 C-elements.

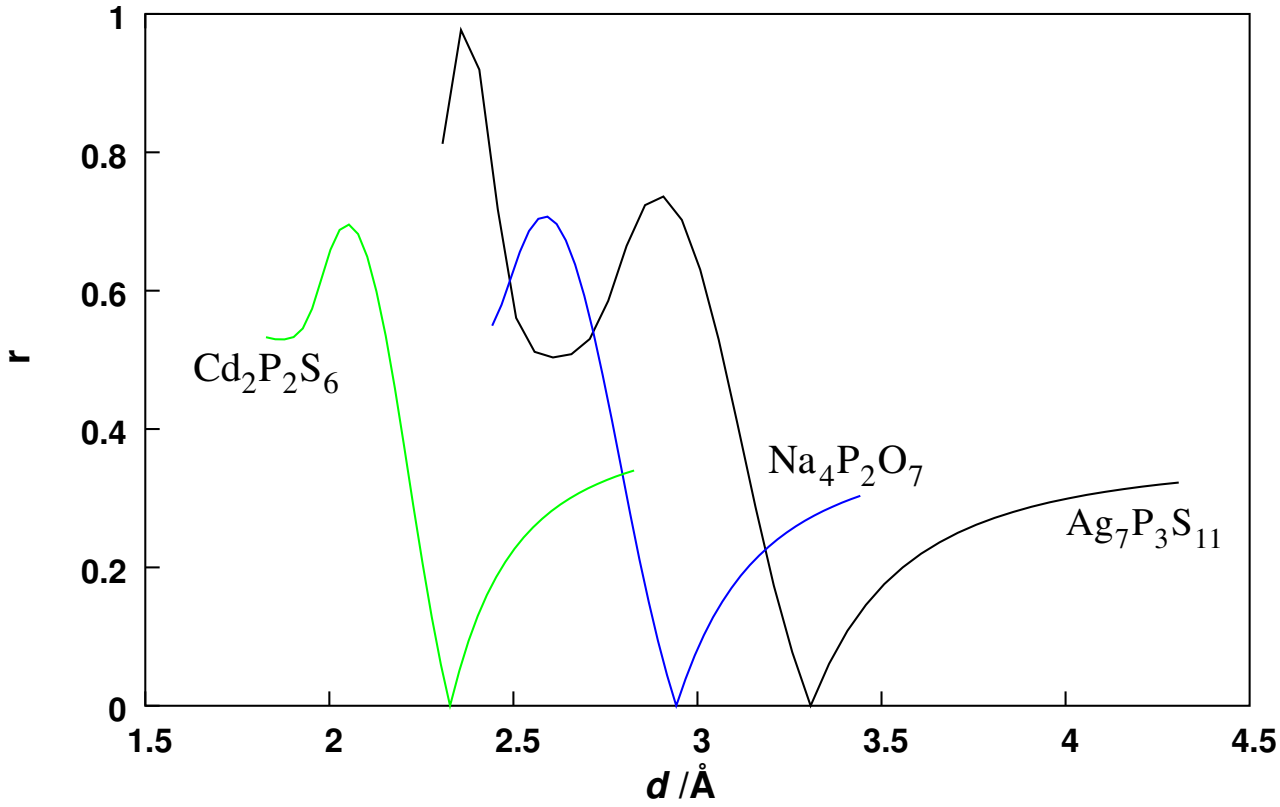

Figure 13: Root mean square deviation r between a DQ constant-time build-up curve with a fixed internuclear distance d_{fixed} and DQ constant-time curve calculated for an internuclear distance d; the root mean square deviation becomes zero if d_{fixed} equals d; shown are three curves with d_{fixed} being chosen as the measured distances for the three model compounds $Cd_2P_2S_6$, $Na_4P_2O_7$ and $Ag_7P_3S_{11}$ by constant-time DQ NMR (Table 4).